

Accepted for publication in the *Astronomical Journal*

A Hubble Space Telescope Snapshot Survey¹ of Dynamically Close Galaxy Pairs in the CNOC2 Redshift Survey

D. R. Patton², J. K. Grant², L. Simard³, C. J. Pritchett⁴, R. G. Carlberg⁵, & K. D. Borne⁶

ABSTRACT

We compare the structural properties of two classes of galaxies at intermediate redshift: those in dynamically close galaxy pairs, and those which are isolated. Both samples are selected from the CNOC2 Redshift Survey, and have redshifts in the range $0.1 < z < 0.6$. Hubble Space Telescope WFPC2 images were acquired as part of a snapshot survey, and were used to measure bulge fraction and asymmetry for these galaxies. We find that paired and isolated galaxies have identical distributions of bulge fractions. Conversely, we find that paired galaxies are much more likely to be asymmetric ($R_T + R_A \geq 0.13$) than isolated galaxies. Assuming that half of these pairs are unlikely to be close enough to merge, we estimate that $40\% \pm 11\%$ of merging galaxies are asymmetric, compared with $9\% \pm 3\%$ of isolated galaxies. The difference is even more striking for strongly asymmetric ($R_T + R_A \geq 0.16$) galaxies: $25\% \pm 8\%$ for merging galaxies versus $1\% \pm 1\%$ for isolated galaxies. We find that strongly asymmetric paired galaxies are very blue, with rest-frame $B - R$ colors close to 0.80, compared with a mean

¹ Based on observations made with the NASA/ESA Hubble Space Telescope, obtained at the Space Telescope Science Institute, which is operated by the Association of Universities for Research in Astronomy, Incorporated, under NASA contract NAS 5-26555.

²Department of Physics, Trent University, 1600 West Bank Drive, Peterborough, ON, K9J 7B8, Canada; dpatton@trentu.ca

³Herzberg Institute of Astrophysics, National Research Council of Canada, 5071 West Saanich Road, Victoria, BC, V9E 2E7, Canada

⁴Department of Physics and Astronomy, University of Victoria, PO Box 3055 STN CSC, Victoria, BC, V8W 3P6, Canada

⁵Department of Astronomy & Astrophysics, University of Toronto, 60 St. George Street, Toronto, ON, M5S 3H8, Canada

⁶George Mason University, School of Computational Sciences, MS 5c3, 4400 University Dr., Fairfax, VA 22030, USA

$(B - R)_0$ of 1.24 for all paired galaxies. In addition, asymmetric galaxies in pairs have strong $[\text{OII}]3727\text{\AA}$ emission lines. We conclude that close to half of the galaxy pairs in our sample are in the process of merging, and that most of these mergers are accompanied by triggered star formation.

Subject headings: galaxies: evolution, galaxies: interactions, galaxies: structure, surveys

1. Introduction

Observational studies of galaxy interactions and mergers have a long history, beginning with the identification of a sample of close galaxy pairs by Holmberg (1937). Detailed multi-wavelength observations of nearby pairs such as the Antennae (NGC 4038/4039) yield strong evidence for ongoing mergers, including tidal tails, induced star formation, and multiple nuclei. Hierarchical models of galaxy formation indicate that mergers and accretion events play a key role in building up the galaxy populations we see today (Coles 2005).

There is growing interest in quantifying the contribution that mergers have played in forming the galaxies we see in the nearby universe. Recent efforts have focussed on two central questions: (1) how often do mergers take place? and (2) what effects do mergers have on the constituent galaxies? The answers to both questions are certain to vary with cosmic time, and therefore require the observation of merging systems at a wide range of redshifts. In this paper, we analyze Hubble Space Telescope (hereafter HST) images of a sample of galaxy pairs at intermediate redshifts, with the goal of shedding new light on both issues at a lookback time of several gigayears.

Attempts to address the first question have centred on measurement of the galaxy merger rate, and its evolution with redshift. In recent years, many of these studies have used close galaxy pairs to identify systems in which mergers are imminent (Patton et al. 2000; Le Fèvre et al. 2000; Carlberg et al. 2000; Patton et al. 2002; Bundy et al. 2004; Lin et al. 2004). The number of close companions per galaxy is taken to be proportional to the galaxy merger rate. Alternatively, one can identify merging systems using quantitative measurements of galaxy asymmetries (Conselice et al. 2003 and references therein). The resulting merger fraction is assumed to be proportional to the galaxy merger rate. These two methods are independent and complementary. Close galaxy pairs probe early stage mergers, while strong asymmetries are more likely to identify later stage mergers, including merger remnants. There should be considerable overlap between these samples if the galaxy pairs are close enough to include strongly interacting systems.

Until now, however, there has been very little evidence to confirm this assumption. Most high redshift pair samples have been identified using ground-based telescopes, and therefore yield minimal morphological information (e.g., Patton et al. 1997). Le Fèvre et al. (2000) did have HST imaging of 285 galaxies at high redshift; however, they had redshifts for only one member of each pair. At low redshift, Patton et al. (2000) estimated that $\sim 30\%$ of their close pairs exhibit convincing evidence of interactions on Digitized Sky Survey images. However, their classifications were made by eye, and therefore difficult to compare with quantitative measurements of asymmetry.

In this study, we aim to rectify these shortcomings by analyzing the structural properties of dynamically close galaxy pairs identified by Patton et al. (2002; hereafter P2002), using high resolution imaging from HST. The following section describes the observations and data reduction, and the identification of paired and isolated galaxies is outlined in § 3. A statistical comparison of the structural parameters of these two samples is provided in § 4. We estimate the asymmetry fraction of paired and isolated galaxies in § 5, and compare their star forming properties in § 6. The results are discussed in § 7, and followed by our conclusions in § 8. For consistency with the sample selection of P2002, we adopt a cosmology of $H_0=100 \text{ km s}^{-1}\text{Mpc}^{-1}$, $\Omega_M = 0.2$, and $\Omega_\Lambda=0$.

2. Observations and Data Reduction

The primary goal of this study is to examine the structural properties of galaxies in merging pairs, and to compare the results with those of isolated galaxies. This requires high resolution imaging of a sample of confirmed close pairs, along with a control sample of field galaxies. In this section, we describe the identification of a sample of dynamically close galaxy pairs from the CNOC2 survey, and the acquisition of HST imaging for a subset of these pairs.

2.1. Dynamical Pairs from the CNOC2 Survey

The CNOC2 Field Galaxy Redshift Survey (Yee et al. 2000) contains redshifts for approximately 6000 galaxies at redshifts of $0.1 < z < 0.6$. Images and spectra were acquired using the multi-object spectrograph (MOS) at the Canada-France-Hawaii Telescope. This survey covers four well-separated patches on the sky, covering 1.5 deg^2 to a depth of $R_C = 21.5$, with an overall spectroscopic completeness of approximately 50%.

P2002 identified a sample of 88 galaxies in dynamically close pairs from the CNOC2

survey, and used these pairs to estimate the galaxy merger and accretion rates at $z = 0.3$. Galaxy pairs were identified using separation criteria (see § 2.2), and without regard to morphology. In fact, very little morphological detail is seen in the short (~ 6 minute) MOS exposures, in which atmospheric seeing blurs out most of the detail in these galaxies.

P2002 argue that roughly half of these pairs are likely to be undergoing mergers. Part of the evidence comes from studying identically selected galaxy pairs at low redshift, using the SSRS2 Redshift Survey (Patton et al. 2000). Clear morphological signs of ongoing interactions are seen in Digitized Sky Survey images of many of these pairs. However, it is unclear if the same systems are likely to be identified in deeper samples such as CNOC2, in part due to increased contamination by unrelated foreground and background galaxies. Moreover, while the qualitative analysis of SSRS2 pairs was intriguing, it would be preferable to quantify morphological signs of interactions in an objective and reproducible manner.

2.2. HST Snapshot Survey

In order to address these issues, we have carried out an HST snapshot survey of dynamically close galaxy pairs from CNOC2. Our full snapshot sample consisted of all CNOC2 pairs satisfying the following two sets of criteria. First, all member galaxies were required to have apparent magnitude $R_C \leq 21.5$, a secure spectroscopic redshift, and absolute magnitude $M_R^{k,e} \leq -17$, where $M_R^{k,e}$ denotes the k -corrected and evolution-corrected ($E(z)=-z$) absolute magnitude in the Cousins R_C filter. In addition, each pair was required to have a projected physical separation less than $20 h^{-1}$ kpc, and a rest-frame relative velocity less than 500 km/s. Approximately half of the pairs in this sample are likely to have true physical separations of less than $20 h^{-1}$ kpc, and are therefore expected to merge within 0.5 Gyr (Patton et al. 1997, 2000).

Using the preliminary CNOC2 catalogs available in advance of the HST observations (February 1999), this yielded a sample of 72 candidate galaxy pairs. CNOC2 astrometry was used to determine the position of the center of each galaxy pair, and the HST imaging was required to have the pair centred on the WF3 CCD, which is relatively free of cosmetic defects. As each targeted pair fits easily within the WF3 chip, no restriction was imposed on the orientation of WFPC2 (this maximizes the number of targets that can be observed in snapshot mode). In § 3.1, we discuss the final sample of dynamically confirmed galaxy pairs used in this study.

WFPC2 snapshot observations for this program (proposal ID 8230; PI Patton) were carried out between July 1999 and June 2001. Of the 72 galaxy pairs in our target list,

44 were observed. For each field, two 500-second F814W images were acquired, in order to facilitate the removal of cosmic rays. The F814W filter corresponds to rest-frame R at the mean redshift of the sample. These images were calibrated “on-the-fly” as they were retrieved from the HST archive. The final images used in this analysis were downloaded from the HST archive in September 2003, to ensure consistent and updated calibrations.

2.3. HST Image Analysis

Each pair of images was co-added with cosmic ray rejection. Object finding was then performed using SExtractor (Bertin & Arnouts 1996), using the same source detection parameters as Simard et al. (2002). Particular care was taken to ensure accurate de-blending of galaxies in close proximity to one another, while avoiding the detection of substructure within individual galaxies. This was achieved by setting the SExtractor DEBLEND_MINCONT parameter to 0.009. All of the object finding was inspected by eye, and confirmed to be successful for all of the bright galaxies on these images, including every galaxy used in the analysis that follows.

Additional preprocessing and image analysis was carried out using the Galaxy Image 2D (GIM2D) software package (Simard 1998; Simard et al. 2002). This IRAF/SPP package performs detailed bulge+disk decompositions of low signal-to-noise images of distant galaxies in a fully automated way, and has a proven track record with HST images (e.g., Tran et al. 2001; Im et al. 2002). GIM2D was used to measure a variety of structural parameters for each galaxy detected in our snapshot survey.

We focus on two specific structural parameters that are best suited to revealing the structures of interest in this study. The first is the bulge fraction (B/T), which describes the overall structure of each galaxy. This parameter is a measure of the fraction of the galaxy light attributed to the bulge component. This quantity is determined using bulge+disk decomposition. A pure disk system has $B/T=0$, and a pure bulge system has $B/T=1$.

The second structural parameter we employ is asymmetry, which is used to detect morphological signs of interactions that may be present. While GIM2D makes several measurements of asymmetry, we choose to use $R_T + R_A$, which is a measure of the overall smoothness of the galaxy image with respect to the bulge+disk model. R_T and R_A are defined in equation 11 of Simard et al. (2002), and are the GIM2D versions of the parameters originally introduced by Schade et al. (1995). R_T and R_A are approximately equal to the total and asymmetric residual flux respectively, and are expressed as a fraction of the total galaxy flux. The discriminating power of $R_T + R_A$, as computed by GIM2D, has been demonstrated by

Im et al. (2002) and McIntosh, Rix, & Caldwell (2004). We compute $R_T + R_A$ within two half light radii. This region is large enough to sample the vast majority of the asymmetric light in these systems. Using a larger aperture could, in principle, increase contamination due to light from neighbouring galaxies. However, we note that the main conclusions of this study are unchanged by measuring asymmetry within three, four, or five half light radii. We conclude that this asymmetry parameter should be sensitive to the most significant morphological signs of interactions that are present in this sample.

3. Extraction of Paired and Isolated Galaxies

3.1. Paired Galaxy Sample

In this section, we describe the identification of a secure sample of paired galaxies found on the HST images. All 44 images were inspected visually to confirm the presence of a galaxy pair at the expected location (the centre of the WF3 CCD). In one instance, a single galaxy was found (Target 64). In this case, it appears that the ground-based CNOC2 survey mistakenly identified a bright region within a galaxy as a separate galaxy. In addition, revised redshift measurements in the final CNOC2 catalog led to the removal of two pairs (Targets 03 and 71) from the sample, as their member galaxies are no longer found to be at similar redshifts. Three pairs (Targets 22, 23, and 43) were known in advance to have only a single redshift, and hence were discarded from this pairs sample. Finally, given that pairs with widely differing masses are less likely to exhibit interaction-induced structural changes, a restriction of 2.5 magnitudes difference in absolute magnitude was imposed. This removed three additional pairs (Targets 02, 62, and 63) from the sample.

We are left with a sample of 35 dynamically close galaxies pairs in these HST images, containing 70 paired galaxies. We note that our definition of a close companion allows for triples and higher order groupings; however, the original snapshot sample included only one triple, and this system was not observed with HST. The basic properties of the pairs are listed in Table 1, including: HST Target number, mean redshift, angular separation (θ), projected physical separation (r_p), rest-frame relative velocity (Δv), and difference in absolute magnitude (ΔM_R). We note that some of these pairs have slightly different projected separations than reported by P2002. due to improved angular pair separation measurements from HST imaging.

WFPC2 F814W postage stamp images of the galaxies in these pairs are presented in Figure 1. Table 2 contain properties of these paired galaxies, including: HST ID (HST Target; galaxy A or B), CNOC2 name (patch and serial number), HST astrometry (J2000),

spectroscopic redshift, apparent magnitude in Cousins R , and absolute magnitude in Cousins R (M_R). Additional properties given in these tables are described later in the paper.

3.2. Control Sample

While this snapshot survey targeted galaxy pairs, many other CNOC2 galaxies are found on these WFPC2 images. This allows for the identification of a control sample of field galaxies at similar redshifts. This is an *essential* component of this analysis, as it enables us to determine if paired galaxies differ significantly from isolated field galaxies.

We require the control sample to be chosen in precisely the same manner as paired galaxies, with the exception of the requirement of a dynamically close neighbour. Of greatest importance is the availability of a spectroscopic redshift from CNOC2, so as to ensure a fair comparison with the pair sample, and to confirm isolation. We then apply identical apparent and absolute magnitude cuts as for the paired galaxies: namely, $R_C < 21.5$ and $M_R^{k,e} \leq -17$. These redshift catalogs were cross-correlated with the HST images, in order to identify candidates for the control sample. Any galaxies lying too close to the edges of the WF chips were excluded from the analysis. In addition, a number of galaxy images were adversely affected by bad columns on the CCDs, preventing accurate measurement of structural parameters; hence they too were removed from the control sample (note that this did not happen with any of the paired galaxies, since all pairs were centred on a clean region in the center of the WF3 chip). This yielded a control sample of 157 field galaxies.

3.3. Isolated Galaxy Sample

As stated earlier, the primary goal of this study is to determine what effect (if any) the presence of a close companion has on a paired galaxy. To this end, we would ideally like to compare the paired galaxy sample with field galaxies which are certain to have no close companions. A cursory inspection of the control sample reveals that in fact many of these galaxies do appear to have relatively nearby companions. For approximately half of these companions, we can use their redshifts to determine if they are at a similar redshift or not. For the remainder, the lack of redshift information means that we cannot rule them out as possible physical companions.

With this in mind, we apply several additional criteria to the control sample to ensure that all remaining galaxies are truly isolated. A neighbouring galaxy is initially considered to be a companion if it lies within a projected separation of $40 h^{-1}$ kpc and has an observed

flux larger than 20% (ie., within 1.75 magnitudes) of the host galaxy. Any companion with a rest-frame relative velocity larger than 1000 km/s is discarded. Every galaxy in the control sample which has no companions is then classified as isolated. These criteria yield a sample of 77 isolated galaxies. Postage stamp images of these isolated galaxies are shown in Figure 2. Table 3 contains a list of properties of these galaxies, in the same format as Table 2.

3.4. Redshift Distributions

The redshift-absolute magnitude distributions of paired and isolated galaxies are compared in Figure 3. Overall, these samples are seen to have similar distributions. However, isolated galaxies appear to lie at slightly higher redshifts than paired galaxies. This is a natural consequence of the selection criteria imposed. Optical contamination due to higher redshift interlopers is expected to be higher for galaxies at low redshift, due to the larger angular search area. As a result, it is more difficult to confirm isolation for galaxies at the low redshift end of the sample. In addition, the detection of galaxy pairs depends on the square of the selection function, meaning that pairs will be relatively rare at the high redshift end of the sample (Patton et al. 2000).

However, the difference in mean redshift between paired and isolated galaxies is small (0.03), and is significant only at the 1σ level. Consequently, differences in the redshift distributions of paired and isolated galaxies are unlikely to cause a statistically significant difference in the structural parameters of these samples. Therefore, we ignore this effect throughout the remainder of this paper.

4. Structural Parameters of Paired and Isolated Galaxies

The primary goal of this study is to measure the structural parameters of galaxies in dynamically close galaxy pairs, and to compare these measurements with those of a sample of isolated field galaxies. In the sections that follow, we compare the distributions of B/T and $R_T + R_A$ of paired and isolated galaxies. Table 4 lists these and other statistical properties of paired and isolated galaxies, including the results of KS tests comparing these two samples.

4.1. Bulge Fraction

A histogram of B/T for paired and isolated galaxies is presented in Figure 4. It is immediately apparent that these samples have very similar distributions. We carry out two

tests to verify this statistically. First, we compute the mean of each distribution, along with the error in the mean (see Table 4). The means are found to be statistically identical. Next, we perform a Kolmogorov-Smirnov (K-S) test on the two distributions, in which the K-S probability indicates the significance level for the hypothesis that two samples are drawn from the same distribution. A small significance level indicates that two distributions have significantly different cumulative distribution functions. For the B/T distributions of paired and isolated galaxies, we find a KS probability of 95%, indicating that we do not detect any statistical difference in the samples. Therefore, we conclude that paired and isolated galaxies have statistically equivalent distributions of B/T .

4.2. Asymmetry

A histogram of $R_T + R_A$ for paired and isolated galaxies is presented in Figure 5. These distributions appear to differ substantially, particularly in the high asymmetry regime, where a noticeable tail is seen in the distribution of paired galaxies. This is precisely the regime in which one might expect interacting galaxies to be more prevalent. Table 4 shows that the mean $R_T + R_A$ of paired galaxies is larger than that of isolated galaxies, and the difference is significant at the 1.8σ level. The results of the K-S test confirm this, with a K-S probability of only 16%. We conclude that a subset of the paired galaxies are significantly more asymmetric than isolated galaxies.

4.3. Bulge Fraction versus Asymmetry

In order to better understand these correlations, we investigate the relationship between bulge fraction and asymmetry for paired and isolated galaxies. Figure 6 exhibits several interesting trends. First, for isolated galaxies, there is a small monotonic decrease in asymmetry as bulge fraction increases. The locus of this distribution is similar to that found using galaxies from the Sloan Digital Sky Survey (Abazajian et al. 2004), using identical GIM2D parameters (Simard 2005, in preparation).

This trend is also seen for paired galaxies, though there is much more scatter in the distribution of asymmetries. Overall, paired galaxies appear to have larger asymmetries than isolated galaxies, particularly for low bulge fractions. The most asymmetric paired galaxies ($R_T + R_A > 0.2$) all have low bulge fractions ($B/T < 0.2$). We will investigate the significance of these trends further in § 5.

4.4. Potential Bias Due to Crowding of Galaxies

One possible explanation for the differences seen between paired and isolated galaxies is a bias in the measurement of structural parameters for galaxies which are crowded closely together on the sky. That is, in attempting to measure structural parameters (especially asymmetry) of a given galaxy, it is possible that the measurements may be adversely affected by the presence of a nearby galaxy. In particular, asymmetry measurements could be compromised if the light from a neighbouring galaxy contributes unequal and significant amounts of light to opposite sides of the galaxy in question.

If true, we would expect to see significant trends in observed structural parameters with angular separation of the two galaxies. If this bias is completely responsible for the observed differences between paired and isolated galaxies, we would expect the anomalous paired galaxies to be found preferentially at small angular separations. To investigate this possibility, we plot the structural parameters of paired galaxies versus the angular separation, in Figure 7. No significant dependence on θ is seen in this figure. In particular, galaxies with large asymmetries and large bulge fractions are seen at a wide range of angular separations. This supports the assumption that nearby companions do not cause a significant bias in the measurement of structural parameters. Therefore, we ignore this effect throughout the remainder of this paper.

4.5. Dependence on Pair Separation and Luminosity Ratio

Our sample of galaxy pairs spans a small range in both projected separation (r_p) and line of sight velocity difference (Δv). Nevertheless, we now explore the possibility that the structural parameters depend on this separation. Measured structural parameters are plotted versus r_p and Δv in Figures 8 and 9 respectively. No obvious trend is observed. In particular, galaxies with relative large asymmetries and bulge fractions are found over the full range of parameter space explored: namely, $3 h^{-1} \text{ kpc} < r_p < 21 h^{-1} \text{ kpc}$ and $\Delta v < 425 \text{ km/s}$. This is not particularly surprising, given the limited sample size and the relatively small range of pair separations available. Moreover, the use of projected separation (rather than three-dimensional separation) weakens any existing correlation between pair separation and galaxy properties. With a sample spanning greater pair separations, however, one might well expect to see a stronger dependence of structural properties on pair separation (e.g., Hernández-Toledo et al. 2005).

In addition, one might expect structural properties to depend on the relative mass of the galaxies in merging pairs. In particular, equal mass pairs (major mergers) might be expected

to exhibit stronger signs of interactions than pairs with significantly difference masses (minor mergers). We use the difference in absolute magnitude $M_R^{k,e}$ (hereafter ΔM_R) as our best indicator of this ratio. The maximum ΔM_R in our sample is 2.5 (see § 3.1), corresponding to a 1:10 ratio in luminosity. Structural properties are plotted versus ΔM_R in Figure 10. Once again, no strong correlation is seen. This indicates that any merger-induced changes in morphology are seen throughout the full range of mass ratios probed by our sample.

5. The Asymmetry Fraction

One of the primary goals of this study is to determine whether, and how often, paired galaxies exhibit morphological signs of interactions. To this end, we investigate the fraction of galaxies with measured asymmetry in excess of a given threshold. This approach has been used by Conselice et al. (2003) to estimate the fraction of galaxies undergoing mergers.

We begin by selecting an asymmetry threshold that is likely to distinguish between normal galaxies and those with morphological signs of interactions. Despite the objective and quantitative nature of these asymmetry measurements, the choice of a threshold is somewhat subjective. Images of all of the galaxies in both the paired and isolated samples were inspected by eye, to ascertain whether or not the asymmetries seen were substantial. A threshold of $R_T + R_A = 0.13$ was found to be the best threshold for separating symmetric and asymmetric galaxies. Hereafter, we refer to all galaxies which have $R_T + R_A \geq 0.13$ as being “asymmetric”. This is slightly less strict than the threshold of $R_T + R_A > 0.14$ used by Schade et al. (1995).

Using this definition, we find that $24.3 \pm 5.2\%$ of paired galaxies are asymmetric, compared with $9.1 \pm 3.3\%$ of isolated galaxies. That is, we find that paired galaxies are nearly three times more likely to be classified as asymmetric, and the difference between these samples is significant at the 1.8σ level. A comparison of asymmetry fractions using other choices of thresholds can be seen in the lower panel of Figure 11. This plot reveals a statistically significant difference between the asymmetry fractions of paired and isolated galaxies for a wide range of asymmetry thresholds, strengthening this conclusion.

Moreover, it is important to note that not all galaxies in the paired sample are likely to be undergoing interactions or mergers. Instead, the separation criteria used to identify galaxy pairs are less than perfect at choosing merging pairs, due mainly to the contribution of peculiar velocities to the line-of-sight separation of the galaxies in a given pair. As discussed by Patton et al. (2000), some of the dynamical galaxy pairs identified with these criteria are likely to have true physical separations that are so large that the system will never merge.

The fraction of pairs that are likely to have true three-dimensional physical separations of less than $20 h^{-1}$ kpc has been estimated to be $f_{3D} = 0.5$ (Patton et al. 2000, 2002). While this estimate is approximate in nature, it is greatly preferable to assuming that all of the paired galaxies in our study are close enough to merge.

With this assumption, we infer that our sample of paired galaxies is made up of equal parts isolated galaxies and merging galaxies. Using this approach, we find that $39.5 \pm 10.9\%$ of merging galaxies are asymmetric. This is 4.3 times larger than the asymmetry fraction of isolated galaxies. In the upper panel of Figure 11, the asymmetry fraction of merging and isolated galaxies is plotted over a wide range in asymmetry thresholds. This figure shows that the difference between the two samples is striking, and is not confined to our specific choice of asymmetry threshold. We note also that this result has implications for the K-S test applied to the paired and isolated samples in § 4.2; that is, the K-S probability of 16% is almost certainly too high, due to the mixture of merging and isolated galaxies in the paired sample. We conclude that merging galaxies are significantly more asymmetric than isolated galaxies.

Finally, we repeat this analysis using a stricter asymmetry threshold. Visual inspection of the images indicates that galaxies with $R_T + R_A \geq 0.16$ may be described as “strongly asymmetric”. With this definition, we find that $1.3 \pm 1.3\%$ of isolated galaxies are strongly asymmetric, $12.9 \pm 4.0\%$ of paired galaxies are strongly asymmetric, and $24.5 \pm 8.1\%$ of merging galaxies are strongly asymmetric. Clearly, the difference between the samples is even more striking when the most strongly asymmetric galaxies are considered.

6. Colors and Emission Line Strengths

6.1. Rest-Frame Colors

Historically, there have been many attempts to detect enhanced star formation in merging galaxies (e.g., Larson & Tinsley 1978). Optical colors of galaxies are known to be useful, though imperfect, indicators of their underlying stellar populations and star-forming histories. The HST imaging used in this study are in a single passband (F814W) only; however, we do have integrated color measurements from the CNOC2 survey (Yee et al. 2000). Rest-frame colors were computed by fitting model spectral energy distributions to the CNOC2 photometry ($UBVR_CI_C$). We limit our analysis to rest-frame $B-R$ color, hereafter $(B-R)_0$. The mean colors and cumulative distributions of paired and isolated galaxies are found to be statistically equivalent (see Table 4).

We now investigate the connection between rest-frame colors and structural parameters.

Figure 12 contains a plot of rest-frame color versus bulge fraction, for paired and isolated galaxies. A clear correlation is seen for isolated galaxies, in that galaxies with larger bulge fractions are redder. This result is consistent with numerous studies of the properties of field galaxies (e.g., Roberts & Haynes 1994). A similar correlation is seen for paired galaxies, though there is significantly more scatter in color. Disk-dominated ($B/T < 0.5$) paired galaxies have the same mean color as their isolated counterparts, whereas bulge-dominated paired galaxies are bluer (at the 1.3σ level). If we instead treat bulge fraction as the dependent variable, we find that the bluest paired galaxies ($(B - R)_0 < 1$) have higher bulge fractions than the bluest isolated galaxies (significant at 1.5σ). These results are consistent with a scenario in which mergers have induced central starbursts in some paired galaxies, making them bluer and/or boosting their measured bulge fractions.

In Figure 13, rest-frame color is plotted versus asymmetry. Isolated galaxies exhibit a gradual trend towards larger asymmetry for bluer galaxies, consistent with the color-asymmetry relationship reported by Conselice, Bershadsky, & Jangren (2000) for the Frei et al. sample of (non-merging) nearby galaxies. The mean colors of paired and isolated galaxies are statistically equivalent for systems classified as symmetric ($R_T + R_A < 0.13$). On the other hand, the seven most asymmetric galaxies are all paired, and are very blue ($(B - R)_0 < 0.95$). These galaxies lie in a location on the color-asymmetry plot similar to that of the merger/interaction induced starburst galaxies of Conselice, Bershadsky, & Gallagher (2000). It appears, therefore, that the sample of paired galaxies identified in our study is made up of two subsets: symmetric galaxies with colors identical to isolated galaxies, and asymmetric galaxies with relatively blue colors which have no counterparts in the isolated sample.

6.2. Emission Line Strengths

An independent measure of current star formation can be obtained from the strength of emission line fluxes. The primary emission line detected in the CNOC2 survey (Yee et al. 2000) is $[\text{OII}]3727\text{\AA}$. The rest-frame equivalent width of this line, denoted $\text{EW}([\text{OII}])$, was measured for most of the galaxies of interest in this HST study. Negative $\text{EW}([\text{OII}])$ refers to emission. Strong $[\text{OII}]$ emission is generally associated with current star formation activity (e.g., Kennicutt 1998).

The mean $\text{EW}([\text{OII}])$ is more negative for paired galaxies than isolated galaxies, though the difference is relatively small (5\AA). A K-S test indicates significant differences between the parent distributions. This difference in cumulative distributions appears to originate in the strong emission line regime. In particular, for galaxies with $\text{EW}([\text{OII}]) < -25\text{\AA}$, paired

galaxies outnumber isolated galaxies two to one, despite a slightly smaller sample of paired galaxies versus isolated galaxies. These conclusions are similar to those of Liu & Kennicutt (1995), who compared the spectrophotometric properties of merging and isolated galaxies at low redshift.

In order to see how emission line strength relates to structural parameters, we plot $EW([OII])$ versus bulge fraction (Figure 14) and asymmetry (Figure 15), for both paired and isolated galaxies. While isolated and paired galaxies both exhibit a general trend towards stronger [OII] emission with smaller bulge fraction, paired galaxies are seen to have emission that is stronger than isolated galaxies of the same bulge fraction. Figure 15 shows that the subset of paired galaxies which are asymmetric exhibit strong [OII] emission. In addition, direct comparison of colors and emission lines for individual galaxies reveals that, for the sample of 8 strongly asymmetric paired galaxies in Figure 13, 4/4 galaxies with emission line measurements have strong emission ($EW([OII]) < -27\text{\AA}$). These results are broadly consistent with the conclusions of the previous section.

7. Discussion

7.1. Does the Observed Asymmetry Fraction Make Sense?

In § 5, we estimated that roughly 40% of galaxies in merging pairs are asymmetric, and 25% are strongly asymmetric. While these fractions are much higher than the equivalent measurements for isolated galaxies, it is worth investigating if these results are consistent with our hypothesis that the galaxies in our “merging pair” sample are in fact undergoing mergers at the present time. If true, what fraction of these galaxies would be expected to exhibit significant asymmetries? There are several reasons why this fraction is likely to be substantially less than 100%. First, even if these pairs are likely to merge soon, some may be too early in the merging process for strong asymmetries to have been produced. Also, some galaxies (early types in particular) are less likely to exhibit signs of asymmetries than others. Finally, the details of the orbits and galaxy rotations affect the resulting asymmetries. It is therefore difficult to predict in advance what the asymmetry fraction should be.

We can, however, compare with other observations. Conselice (2003) studied a sample of 66 ultraluminous infrared galaxies (ULIRG’s), whose infrared emissions are thought to have been triggered by strong interactions or mergers of gas-rich spiral galaxies (Sanders & Mirabel 1996). Their sample would be expected to exhibit stronger asymmetries than virtually any other sample of galaxies, including the close pairs targeted in this study. They found that approximately 50% of ULIRGs have asymmetries consistent with being involved in

ongoing major mergers. They speculate that the remaining 50% of their sample is composed of systems that are in either the beginning or the end stages of the merger event, when asymmetry is not expected to be strong. Given this result, we conclude that our asymmetry fractions for close galaxy pairs are broadly consistent with the hypothesis of P2002 that approximately 50% of the dynamical pairs identified in this study are currently undergoing mergers.

7.2. Enhanced Star Formation

One of the primary goals of modern day cosmology is the determination of the star formation history of the universe. Numerous studies, beginning with Madau et al. (1996) and Lilly et al. (1996), have shown that the cosmic star formation rate has decreased by an order of magnitude since $z \sim 1$. A compilation by Hogg (2001) indicates that the star formation rate evolves as $(1 + z)^{2.7 \pm 0.7}$ over this redshift range. It is as yet unclear what is driving this change in star formation rate. One obvious candidate is galaxy mergers, since mergers are known to trigger the formation of new stars in at least some merging systems. Moreover, the merger rate appears to increase with redshift, at a level similar to the increase in the cosmic star formation rate (e.g., Le Fèvre et al. 2000; Patton et al. 2002).

At low redshift, there have been several recent studies in which a clear enhancement in star formation is seen in pairs separated by less than $20 h^{-1}$ kpc (Barton et al. 2000; Lambas et al. 2003; Alonso et al. 2004; Nikolic et al. 2004). At higher redshifts, the results have been less conclusive, primarily due to the increased difficulty of identifying dynamically close galaxy pairs (e.g., Zepf & Koo 1989; Carlberg, Pritchet, & Infante 1994). Using a sample of thirteen dynamical pairs at $z \sim 0.3$, Patton et al. (1997) found that four of these pairs contain galaxies with strong [OII] emission, very blue colors, and low relative velocities. While their ground-based images were of marginal quality, some indications of morphological asymmetry were seen in these four pairs.

In § 6, we found that paired galaxies have different distributions of rest-frame color and emission line strengths than isolated galaxies. In particular, the most asymmetric galaxies have unusually blue colors and strong emission lines, and are found almost exclusively in pairs. These results are consistent with a scenario in which merging has induced star formation in a subset of the pair sample. However, many of the remaining paired galaxies have colors and emission line strengths consistent with isolated galaxies. This is hardly surprising, given that the timescale of induced star formation is likely to be considerably shorter than the merging timescale (cf. Barton Gillespie et al. 2003). Moreover, as outlined in § 5, our sample of dynamical pairs is likely to be a roughly equal mix of merging and non-merging

pairs. As our sample of isolated galaxies contains very few asymmetric galaxies, we infer that most of the asymmetric galaxies in the paired sample are found in merging pairs.

We interpret this as evidence of induced star formation occurring in a significant fraction of merging galaxies at $0.1 < z < 0.6$. We have arrived at this conclusion using a sample containing three times as many dynamical pairs as the Patton et al. (1997) sample, and for which we have made quantitative measurements of asymmetry using high resolution HST imaging.

7.3. The Distribution of Bulge Fraction in Paired Galaxies

In § 4.1, we demonstrated that the bulge fraction distributions of paired and isolated galaxies are identical. One possible interpretation of this result is that galaxies of all morphological types have equal probabilities of being involved in these early-stage mergers, and that their bulge fractions are not significantly altered by the interaction until later in the merging process. However, if these early stage mergers have triggered star formation, as we have argued, one might expect this extra star formation to occur primarily in the nuclei, as predicted by simulations (e.g., Barnes & Hernquist 1996). If so, some paired galaxies might be expected to have boosted B/T values, since bulge+disk decompositions cannot easily distinguish between a bona fide bulge and a nuclear starburst. We would therefore have to conclude that, on average, paired galaxies have lower bulge fractions than isolated galaxies. We are unable to distinguish between these two scenarios with these data. However, in a study of the nuclear morphology in the Toomre sequence of merging galaxies, Laine et al. (2003) find no evidence of elevated nuclear emission, except in the latest stage merging systems. This implies that nuclear star formation may not be a significant factor in our pair sample.

8. Conclusions

Using HST imaging of CNOC2 galaxies at $0.1 < z < 0.6$, we have found clear differences in the structural properties of paired and isolated galaxies. While the distribution of bulge fractions are found to be indistinguishable, striking differences are seen in their asymmetries. Assuming that half of our dynamical pairs are unlikely to be close enough to merge, we estimate that $40\% \pm 11\%$ of merging galaxies are asymmetric, compared with $9\% \pm 3\%$ of isolated galaxies. This difference is even more pronounced when considering strongly asymmetric galaxies ($25\% \pm 8\%$ for merging galaxies versus $1\% \pm 1\%$ for isolated galaxies).

These results imply that many of the dynamically close galaxy pairs identified by P2002 are in fact merging, and provide further support for the use of close dynamical pairs in estimating the galaxy merger rate and its evolution with redshift. Moreover, these results demonstrate for the first time that there is considerable overlap between the two most common methods of estimating the galaxy merger rate: namely, morphological merger fractions and close pair statistics.

We also find clear evidence for a connection between asymmetry and star forming properties in galaxy pairs at intermediate redshift. Strongly asymmetric paired galaxies are found to be very blue, with rest-frame colors in the range $0.65 < (B - R)_0 < 0.95$, compared with a mean color of $(B - R)_0 = 1.24$ for all paired galaxies. In addition, asymmetric galaxies in pairs have strong [OII]3727Å emission lines. Within our sample of 35 galaxy pairs, 15 pairs contain at least one asymmetric galaxy, and at least 70% of the asymmetric galaxies in these pairs show signs of enhanced star formation. We conclude that close to half of the galaxy pairs in our sample are in the process of merging, and that the majority of these merging events are accompanied by triggered star formation. When combined with the observed rise in the galaxy merger rate with redshift, the detection of enhanced star formation in many of these systems implies that mergers are at least partially responsible for the rise in the cosmic star formation rate with redshift.

We thank the referee for comments which significantly improved this manuscript. Support for Proposal number 8230 was provided by NASA through a grant from the Space Telescope Science Institute, which is operated by the Association of Universities for Research in Astronomy, Incorporated, under NASA contract NAS5-26555. Support for JG was provided in part by an operating grant from Trent University. DRP, CJP and RGC acknowledge financial support from the Natural Sciences and Engineering Research Council of Canada.

REFERENCES

- Abazajian, K., et al. 2004, *AJ*, 128, 502
- Alonso, M. S., Tissera, P. B., Coldwell, G., & Lambas, D. G. 2004, *MNRAS*, 352, 1081
- Barnes, J. E. & Hernquist, L. 1996, *ApJ*, 471, 115
- Barton, E. J., Geller, M. J., & Kenyon, S. J. 2000, *ApJ*, 530, 660
- Barton Gillespie, E., Geller, M. J., & Kenyon, S. J. 2003, *ApJ*, 582, 668

- Bertin, E. & Arnouts, S. 1996, *A&AS*, 117, 393
- Bundy, K., Fukugita, M., Ellis, R. S., Kodama, T., & Conselice, C. J. 2004, *ApJ*, 601, L123
- Carlberg, R. G., Pritchet, C. J., & Infante, L. 1994, *ApJ*, 435, 540
- Carlberg, R. G., et al. 2000, *ApJ*, 532, L1
- Coles, P. 2005, *Nature*, 433, 248
- Conselice, C. J., Bershad, M. A., & Jangren, A. 2000, *ApJ*, 529, 886
- Conselice, C. J., Bershad, M. A., & Gallagher, J. S. 2000, *A&A*, 354, L21
- Conselice, C. J. 2003, *ApJS*, 147, 1
- Conselice, C. J., Bershad, M. A., Dickinson, M., & Papovich, C. 2003, *AJ*, 126, 1183
- Hernández-Toledo, H. M., Avila-Reese, V., Conselice, C. J., & Puerari, I. 2005, *AJ*, 129, 682
- Hogg, D. 2001, preprint (astro-ph/0105280)
- Holmberg, E. 1937, *Annals of the Observatory of Lund*, 6, 1
- Im, M., et al. 2002, *ApJ*, 571, 136
- Kennicutt, R. C. 1998, *ARA&A*, 36, 189
- Laine, S., van der Marel, R. P., Rossa, J., Hibbard, J. E., Mihos, J. C., Böker, T., & Zabludoff, A. I. 2003, *AJ*, 126, 2717
- Lambas, D. G., Tissera, P. B., Alonso, M. S., & Coldwell, G. 2003, *MNRAS*, 346, 1189
- Larson, R. B. & Tinsley, B. M. 1978, *ApJ*, 219, 46
- Le Fèvre, O., et al. 2000, *MNRAS*, 311, 565
- Lilly, S. J., Le Fevre, O., Hammer, F., & Crampton, D. 1996, *ApJ*, 460, L1
- Lin, L., et al. 2004, *ApJ*, 617, L9
- Liu, C. T. & Kennicutt, R. C. 1995, *ApJ*, 450, 547
- Madau, P., Ferguson, H. C., Dickinson, M. E., Giavalisco, M., Steidel, C. C., & Fruchter, A. 1996, *MNRAS*, 283, 1388
- McIntosh, D. H., Rix, H., & Caldwell, N. 2004, *ApJ*, 610, 161

- Nikolic, B., Cullen, H., & Alexander, P. 2004, MNRAS, 355, 874
- Patton, D. R., Pritchett, C. J., Yee, H. K. C., Ellingson, E., & Carlberg, R. G. 1997, ApJ, 475, 29
- Patton, D. R., Carlberg, R. G., Marzke, R. O., Pritchett, C. J., da Costa, L. N. & Pellegrini, P. S. 2000, ApJ, 536, 153
- Patton, D. R., et al. 2002, ApJ, 565, 208
- Roberts, M. S., & Haynes, M. P. 1994, ARA&A, 32, 115
- Sanders, D. B. & Mirabel, I. F. 1996, ARA&A, 34, 749
- Schade, D., Lilly, S. J., Crampton, D., Hammer, F., Le Fèvre, O., & Tresse, L. 1995, ApJ, 451, L1
- Simard, L. 1998, in ASP Conf. Ser. 145: Astronomical Data Analysis Software and Systems VII, ed. R. Albrecht, R.N. Hook, & H. A. Bushouse (San Francisco ASP), 108
- Simard, L., et al. 2002, ApJS, 142, 1
- Tran, K. H., Simard, L., Zabludoff, A. I., & Mulchaey, J. S. 2001, ApJ, 549, 172
- Yee, H. K. C., et al. 2000, ApJS, 129, 475
- Zepf, S. E. & Koo, D. C. 1989, ApJ, 337, 34

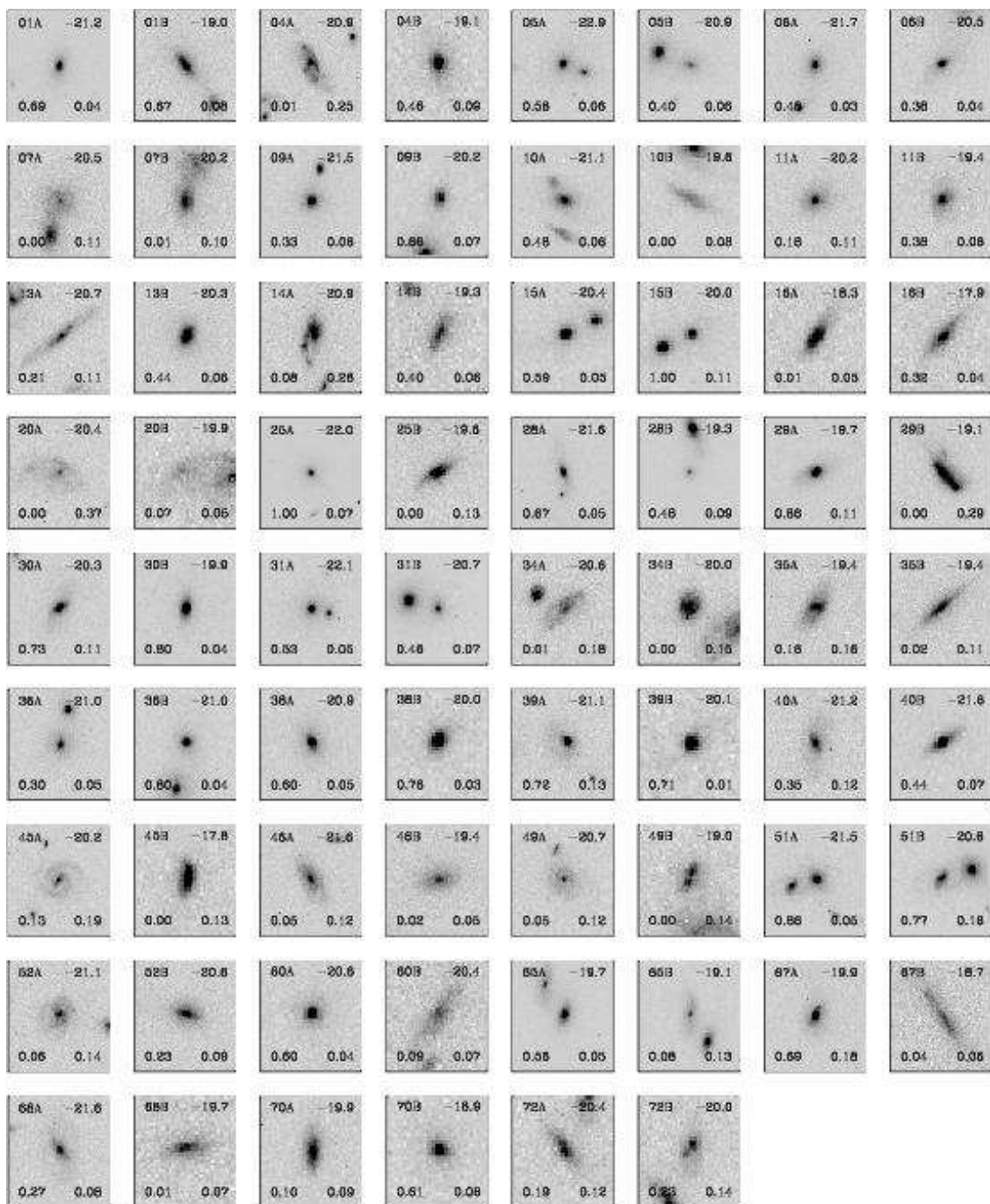


Fig. 1.— Mosaic of the 70 paired galaxies listed in Table 2. Each image is centred on a paired galaxy, and is labelled with: HST ID (upper left), absolute magnitude M_R (upper right), bulge fraction B/T (lower left), and asymmetry $R_T + R_A$ (lower right). The extracted region for each galaxy is 20 times the area of its $1.5\text{-}\sigma_{\text{bkg}}$ isophote. No orientation was specified for these snapshot observations; images therefore have random orientation angles.

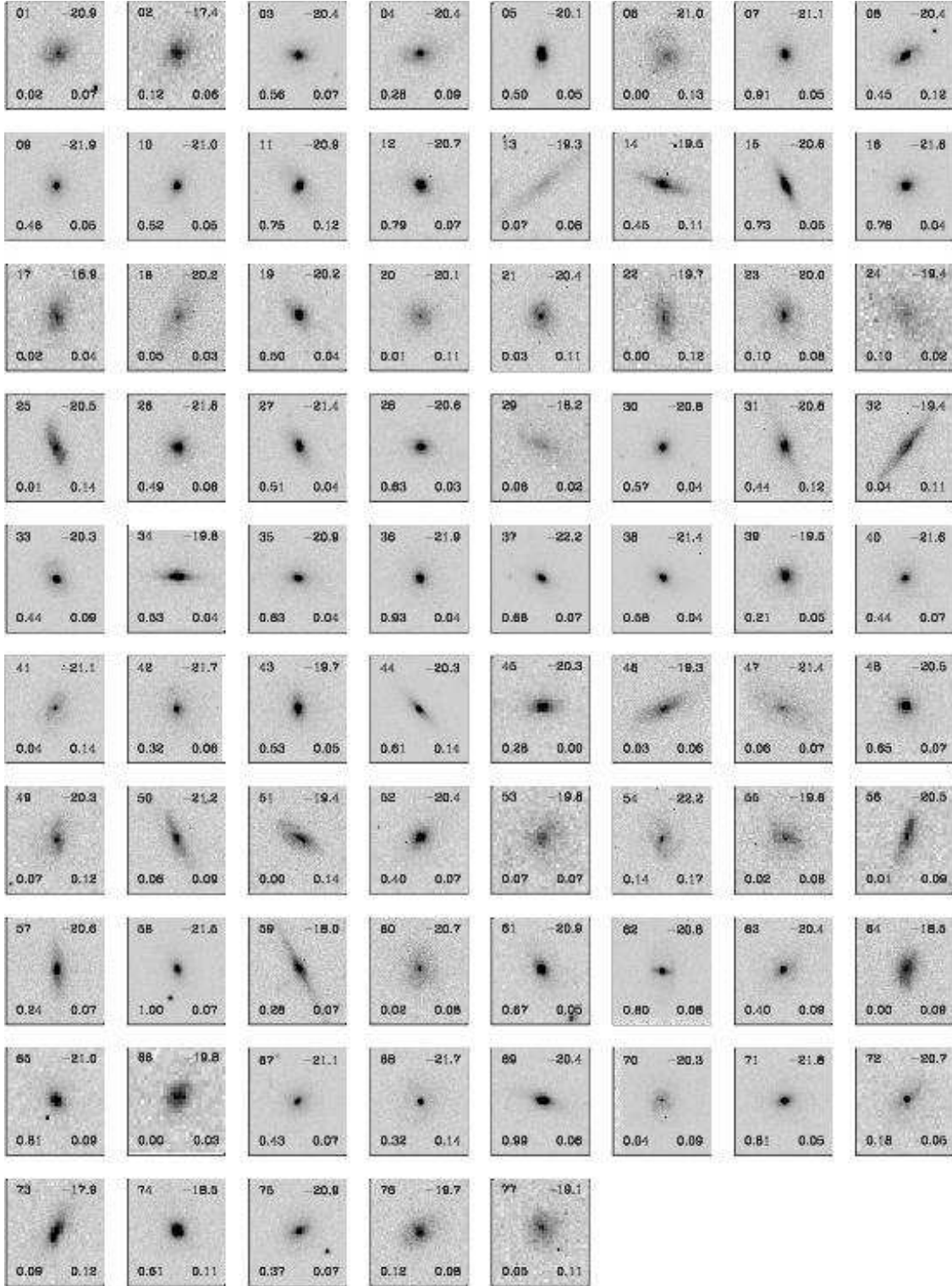


Fig. 2.— Mosaic of the 77 isolated galaxies listed in Table 3. Each image is centred on an isolated galaxy, and has the same labelling and display format as in the preceding figure.

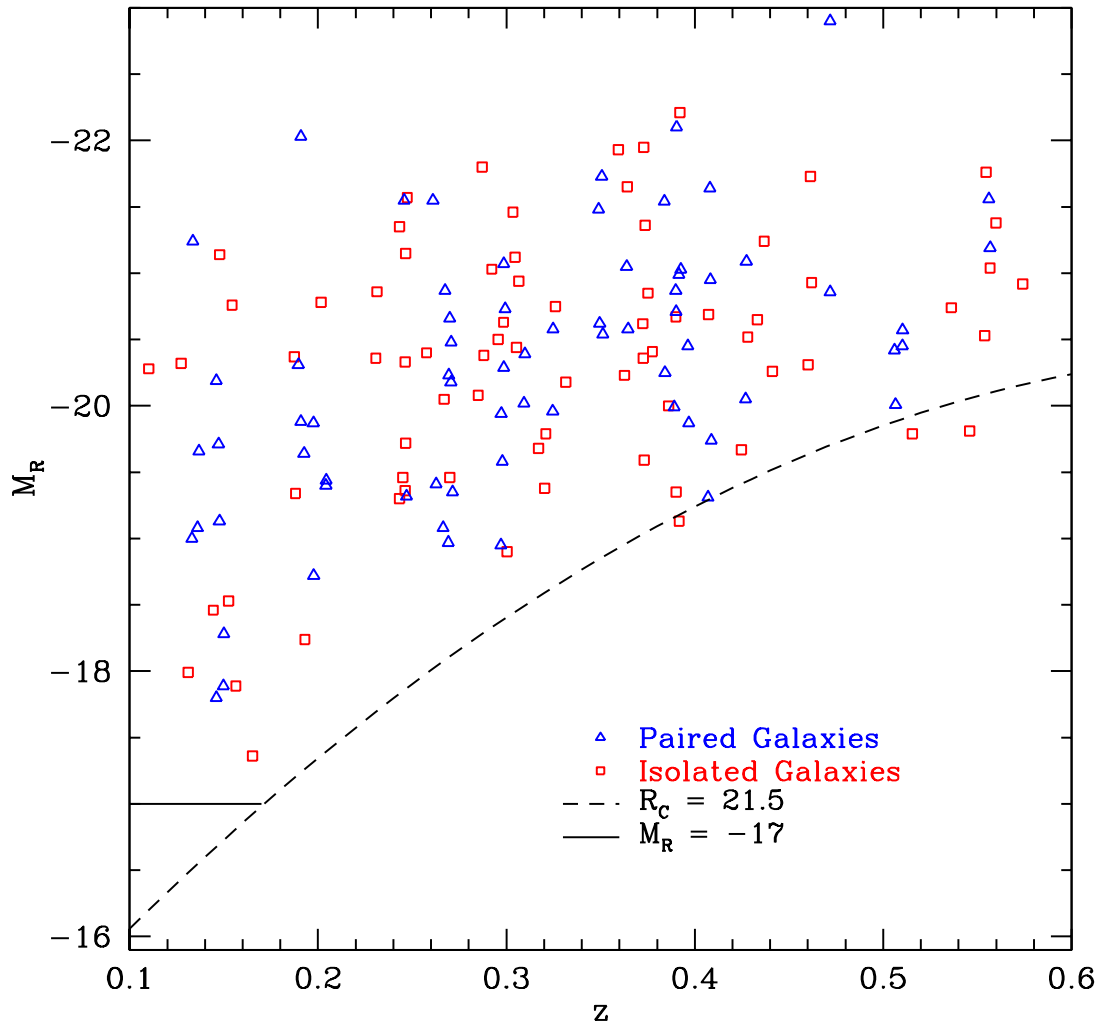


Fig. 3.— Absolute magnitude is plotted versus redshift for paired galaxies (blue triangles) and isolated galaxies (red squares). While the overall distributions of the two samples are similar, isolated galaxies are found at slightly higher redshifts, as expected.

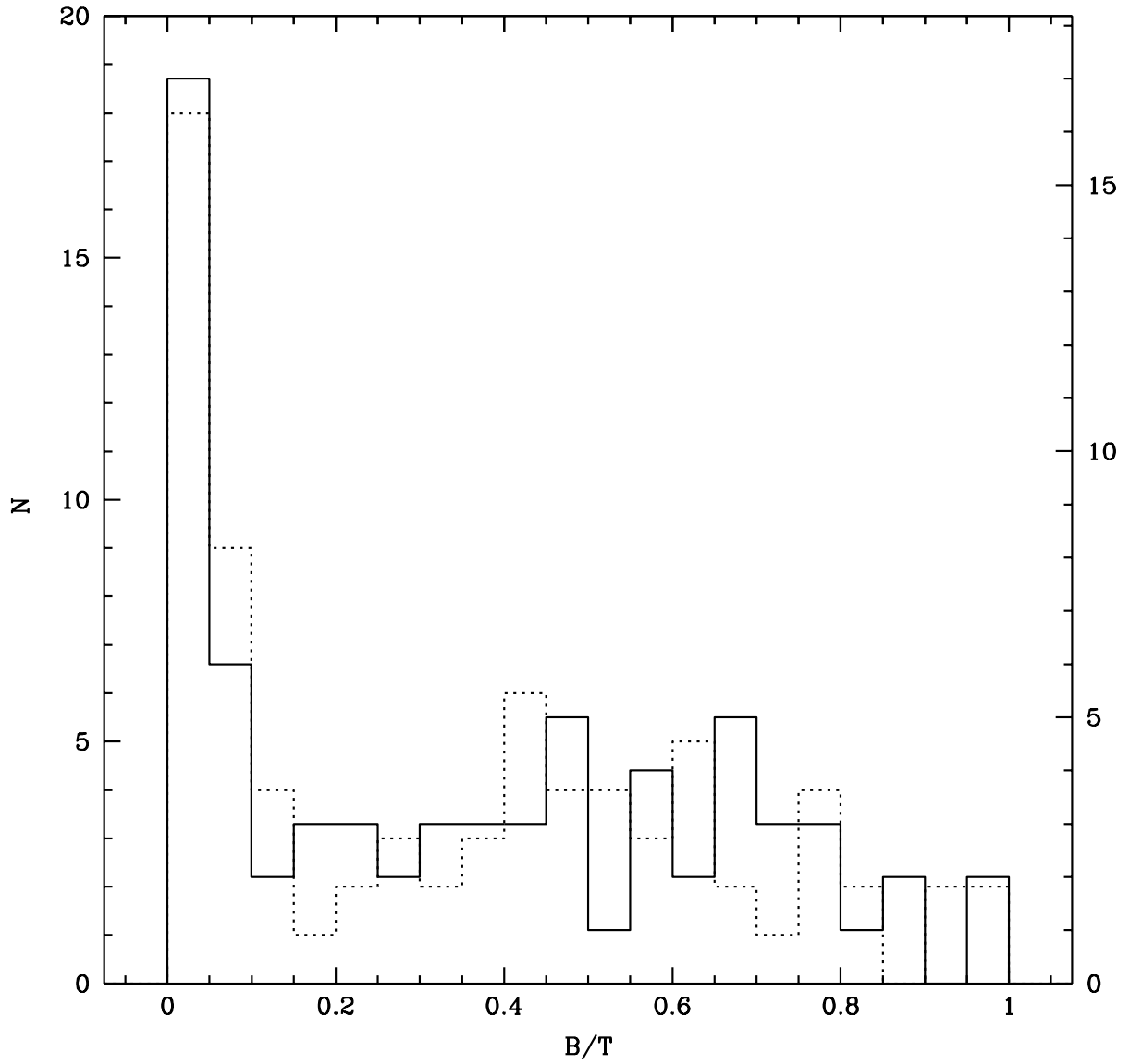


Fig. 4.— Histograms of B/T are given for paired galaxies (solid line) and isolated galaxies (dotted line). The vertical axis on the left gives the number of isolated galaxies, and the vertical axis on the right gives the number of paired galaxies. The histograms have been normalized such that the area under each histogram is the same. No obvious differences are seen in the two distributions.

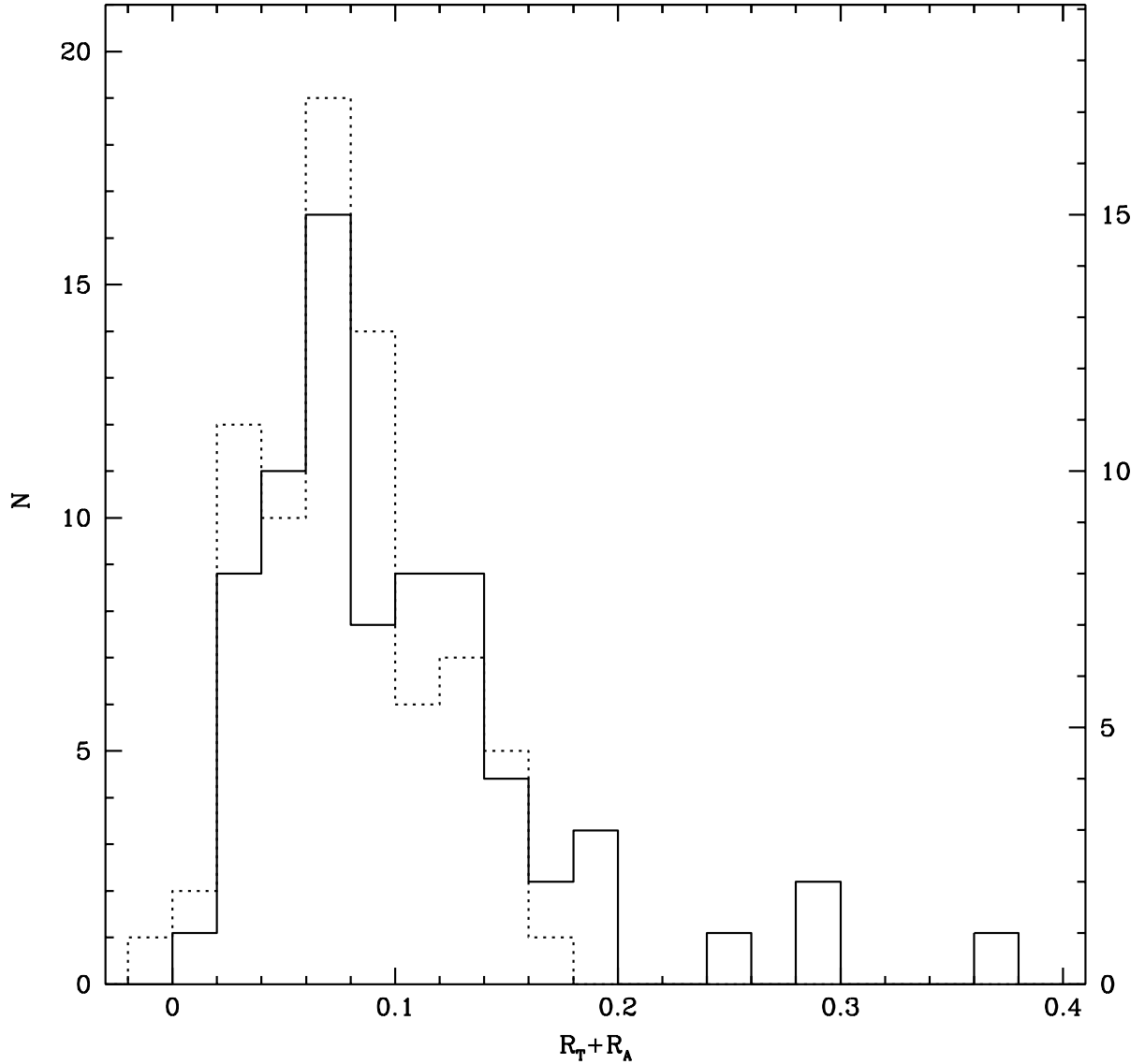


Fig. 5.— Histograms of $R_T + R_A$ are given for paired galaxies (solid line) and isolated galaxies (dotted line). The vertical axis on the left gives the number of isolated galaxies, and the vertical axis on the right gives the number of paired galaxies. The histograms have been normalized such that the area under each histogram is the same. The high asymmetry regime is dominated by paired galaxies.

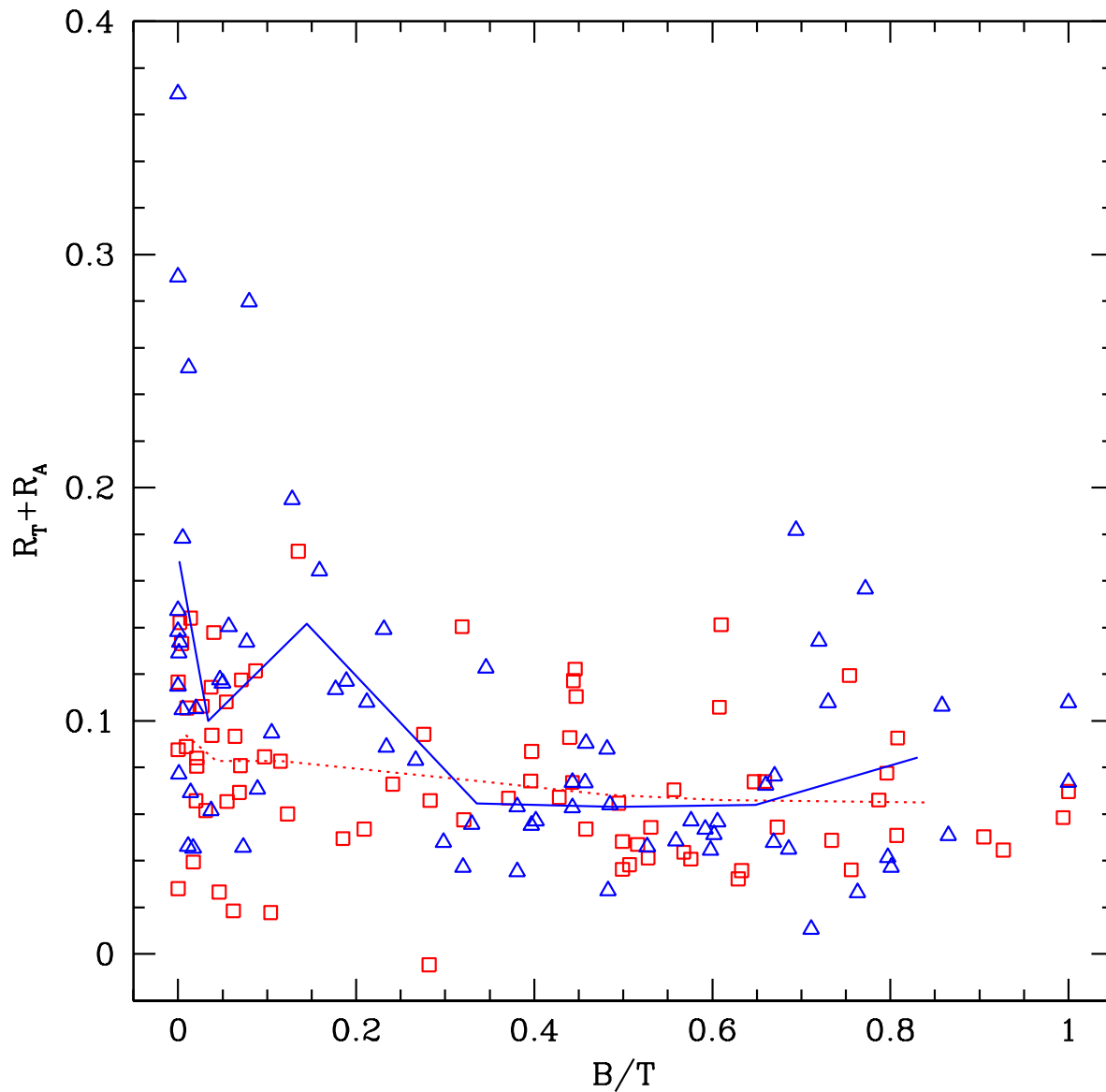


Fig. 6.— Asymmetry is plotted versus bulge fraction for paired galaxies (blue triangles) and isolated galaxies (red squares). The dotted red line gives the mean asymmetry of isolated galaxies in seven bins of B/T , and shows a small decrease of asymmetry with increasing bulge fraction. The solid blue line gives the mean asymmetry of paired galaxies in seven bins of B/T . The most obvious difference between the samples is seen at low bulge fractions, where the mean asymmetry of paired galaxies is noticeably higher than for isolated galaxies.

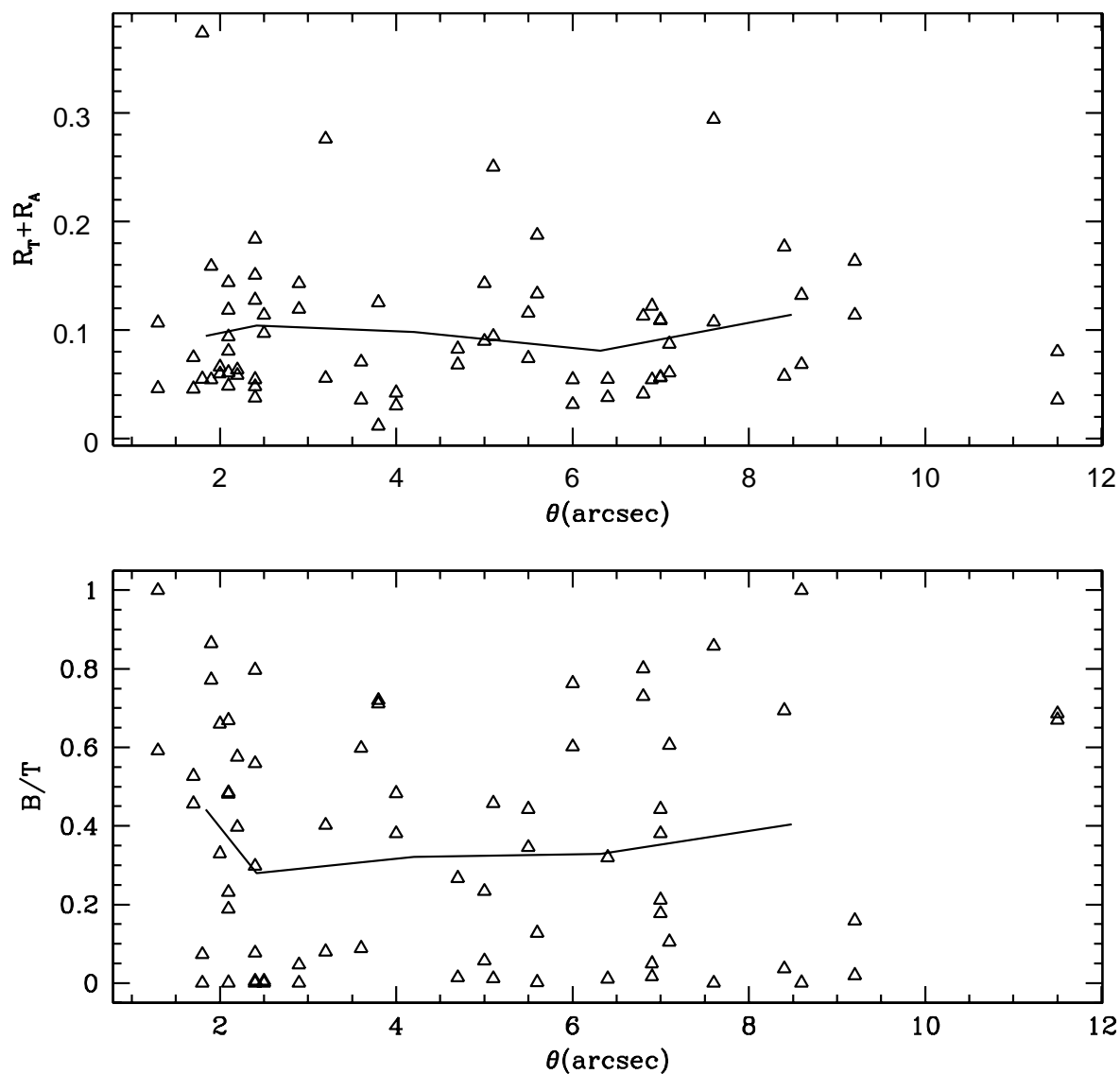


Fig. 7.— Bulge fraction and asymmetry of paired galaxies are plotted versus pair angular separation θ . The solid lines give the mean bulge fraction and asymmetry in five bins of θ (14 galaxies per bin). No significant dependence on θ is seen. This supports the assumption that nearby companions do not cause a significant bias in the measurement of structural parameters.

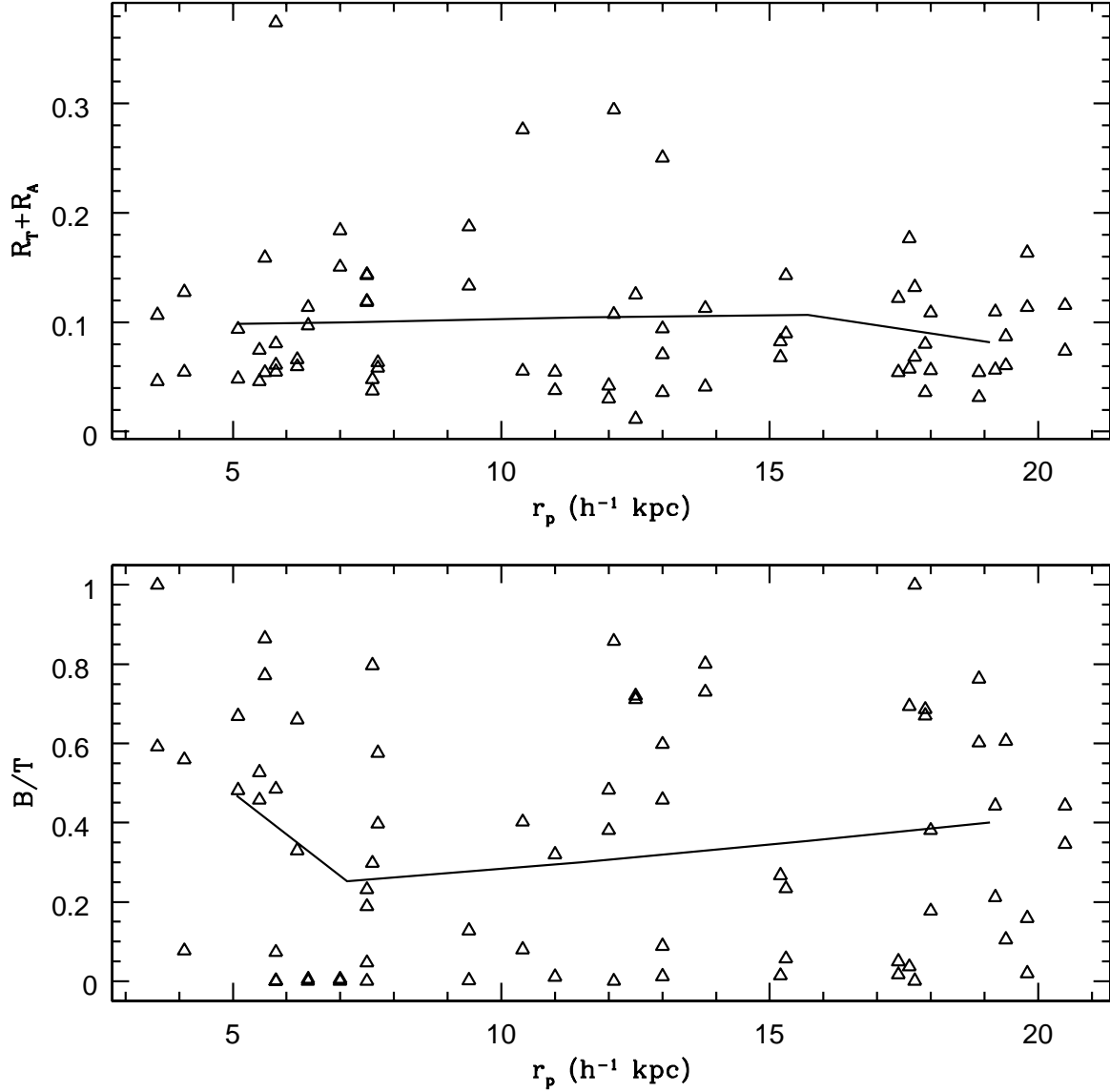


Fig. 8.— Bulge fraction and asymmetry of paired galaxies are plotted versus pair projected physical separation r_p . The solid lines give the mean bulge fraction and asymmetry in five bins of r_p . No significant dependence on r_p is seen.

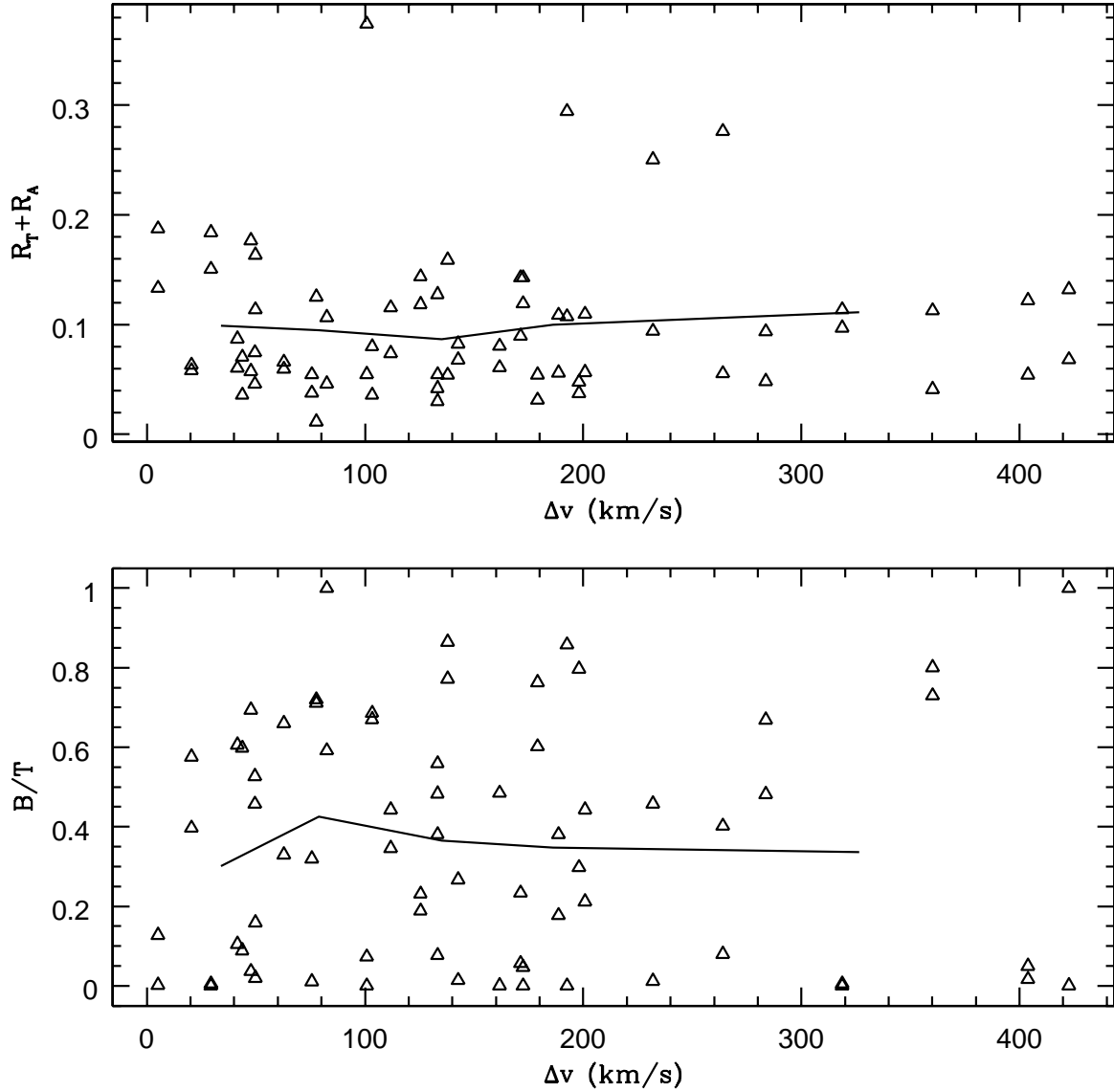


Fig. 9.— Bulge fraction and asymmetry of paired galaxies are plotted versus pair rest-frame relative velocity Δv . The solid lines give the mean bulge fraction and asymmetry in five bins of Δv . No significant dependence on Δv is seen.

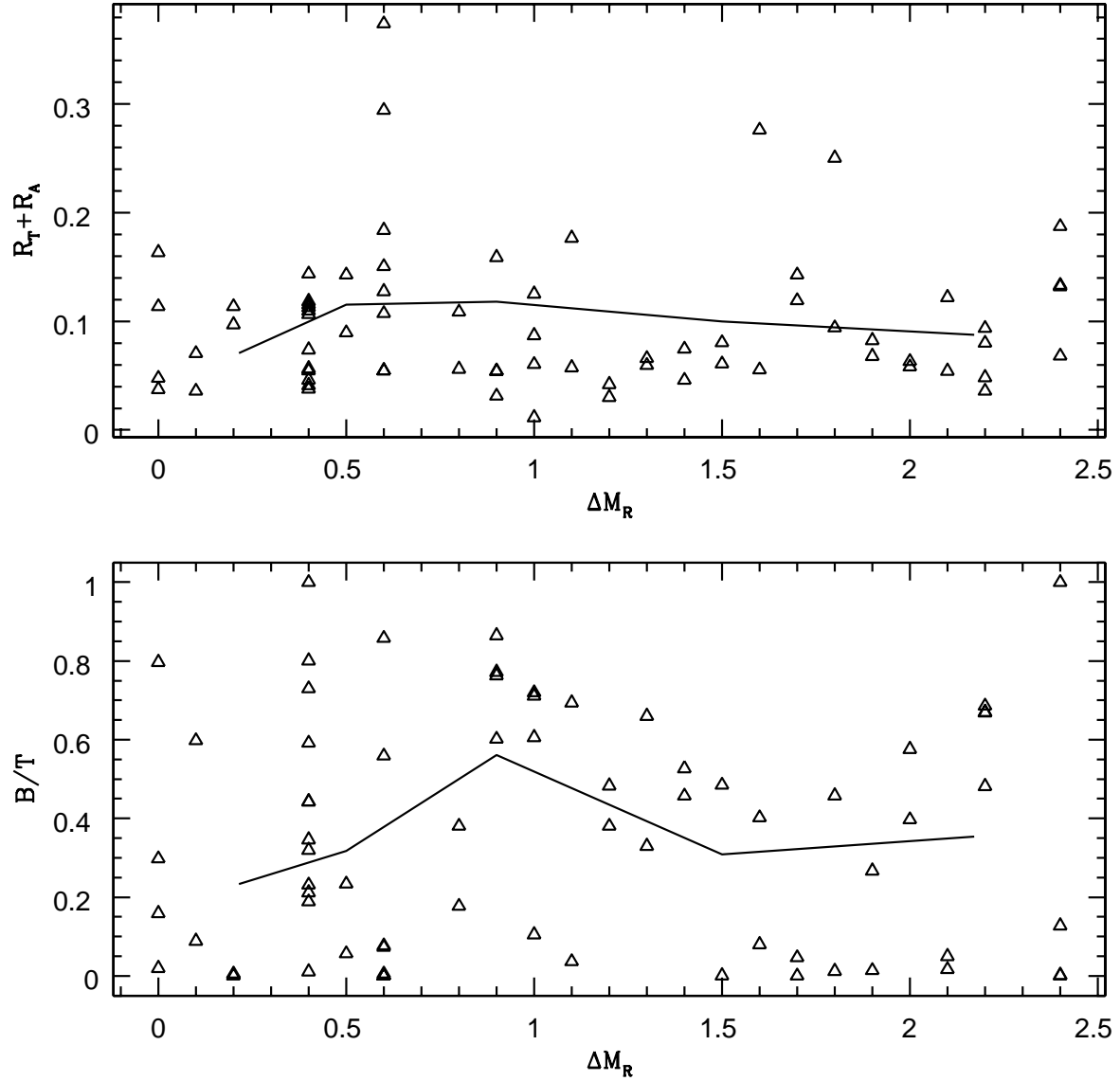


Fig. 10.— Bulge fraction and asymmetry of paired galaxies are plotted versus pair absolute magnitude difference ΔM_R . The solid lines give the mean bulge fraction and asymmetry in five bins of ΔM_R . No significant dependence on ΔM_R is seen.

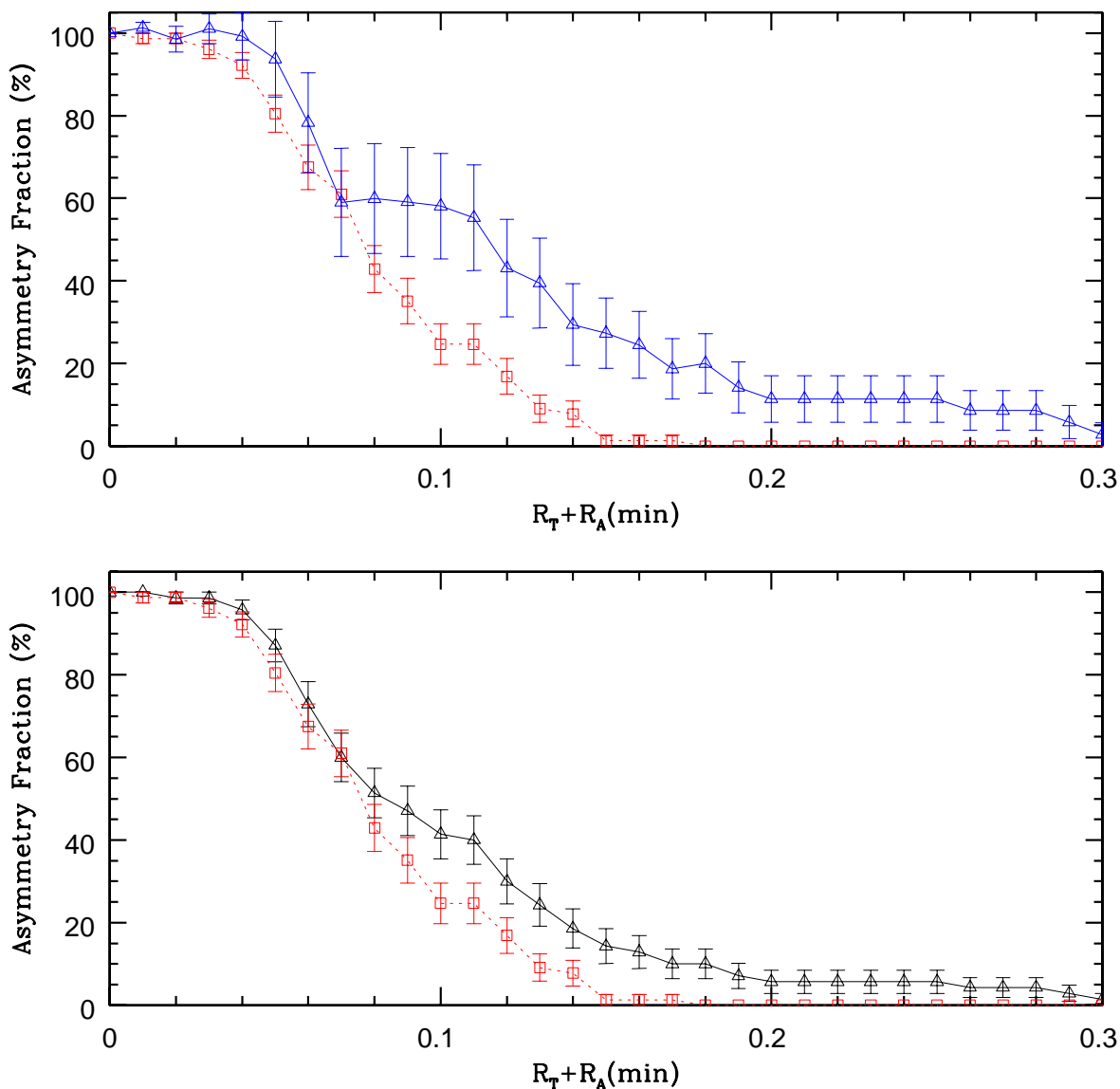


Fig. 11.— The fraction of galaxies more asymmetric than $R_T + R_A$ (min) is plotted versus $R_T + R_A$ (min). (a) The lower plot compares paired galaxies (black triangles connected with a solid line) with isolated galaxies (red squares connected with a dotted line). (b) The upper plot compares “merging” galaxies (blue triangles connected with a solid line) with isolated galaxies (same symbols as lower plot). All error bars are one sigma.

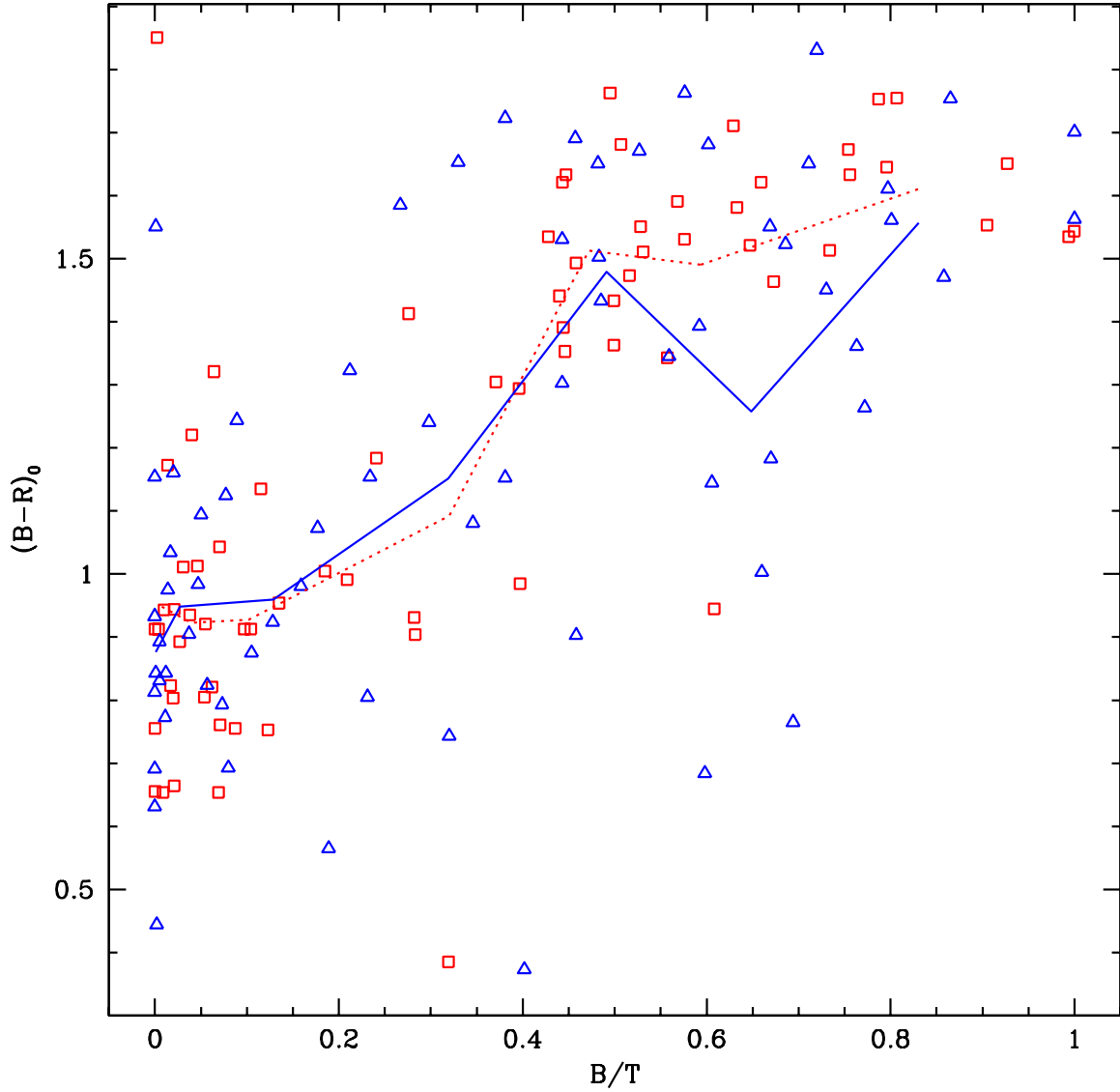


Fig. 12.— Rest-frame $B - R$ color is plotted versus bulge fraction for paired (blue triangles) and isolated (red squares) galaxies. The dotted red line gives the mean color of isolated galaxies in seven bins of B/T , and shows a clear correlation between color and bulge fraction. Similarly, the solid blue line gives the mean color of paired galaxies.

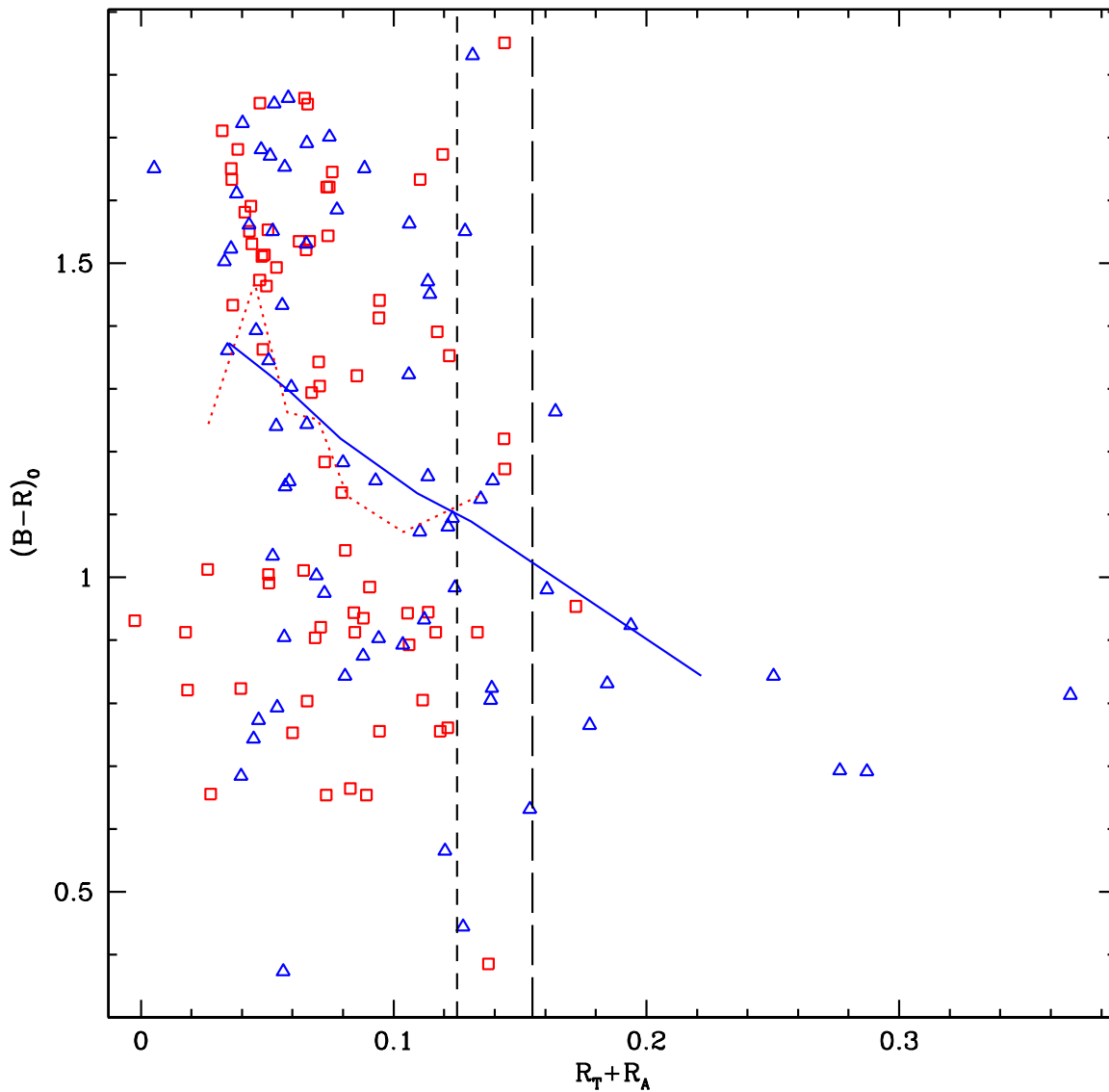


Fig. 13.— Rest-frame $B-R$ color is plotted versus asymmetry for paired (blue triangles) and isolated (red squares) galaxies. Galaxies to the right of the short-dashed line are described as being “asymmetric”; those to the right of the long-dashed line are “strongly asymmetric”. The dotted red line gives the mean color of isolated galaxies in seven bins of $R_T + R_A$, while the solid blue line gives the mean color of paired galaxies. Paired and isolated galaxies have similar distributions in the symmetric regime. Most of the asymmetric galaxies, including the seven most asymmetric galaxies, are blue and found in pairs.

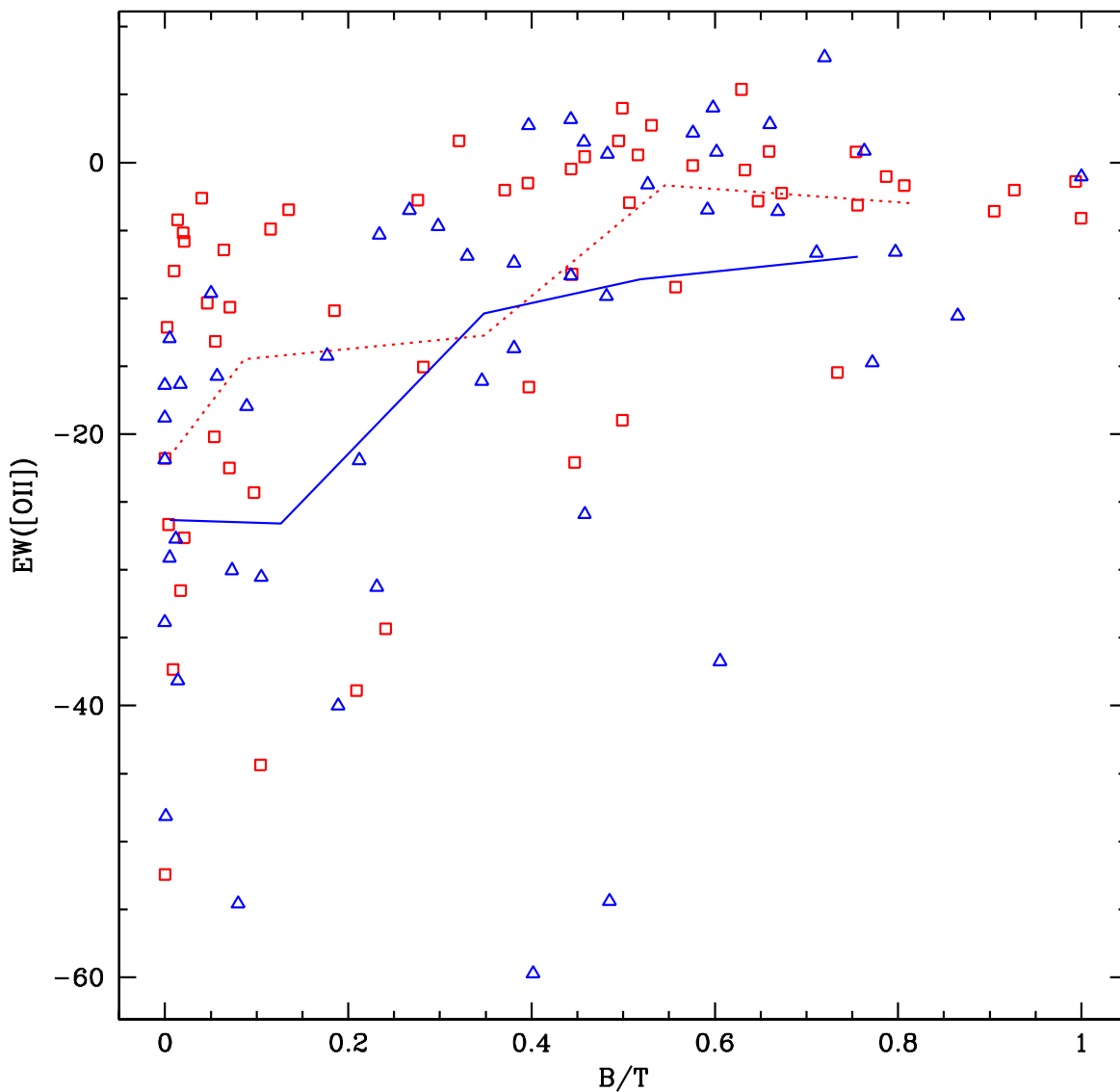


Fig. 14.— $[\text{OII}]3727$ equivalent width is plotted versus bulge fraction for paired (blue triangles) and isolated (red squares) galaxies. The dotted red line gives the mean $\text{EW}([\text{OII}])$ of isolated galaxies in five bins of B/T , and shows an anti-correlation between emission strength and bulge fraction. The solid blue line gives the mean $\text{EW}([\text{OII}])$ of paired galaxies, and exhibits a similar trend. Paired galaxies exhibit stronger emission than isolated galaxies at nearly all bulge fractions.

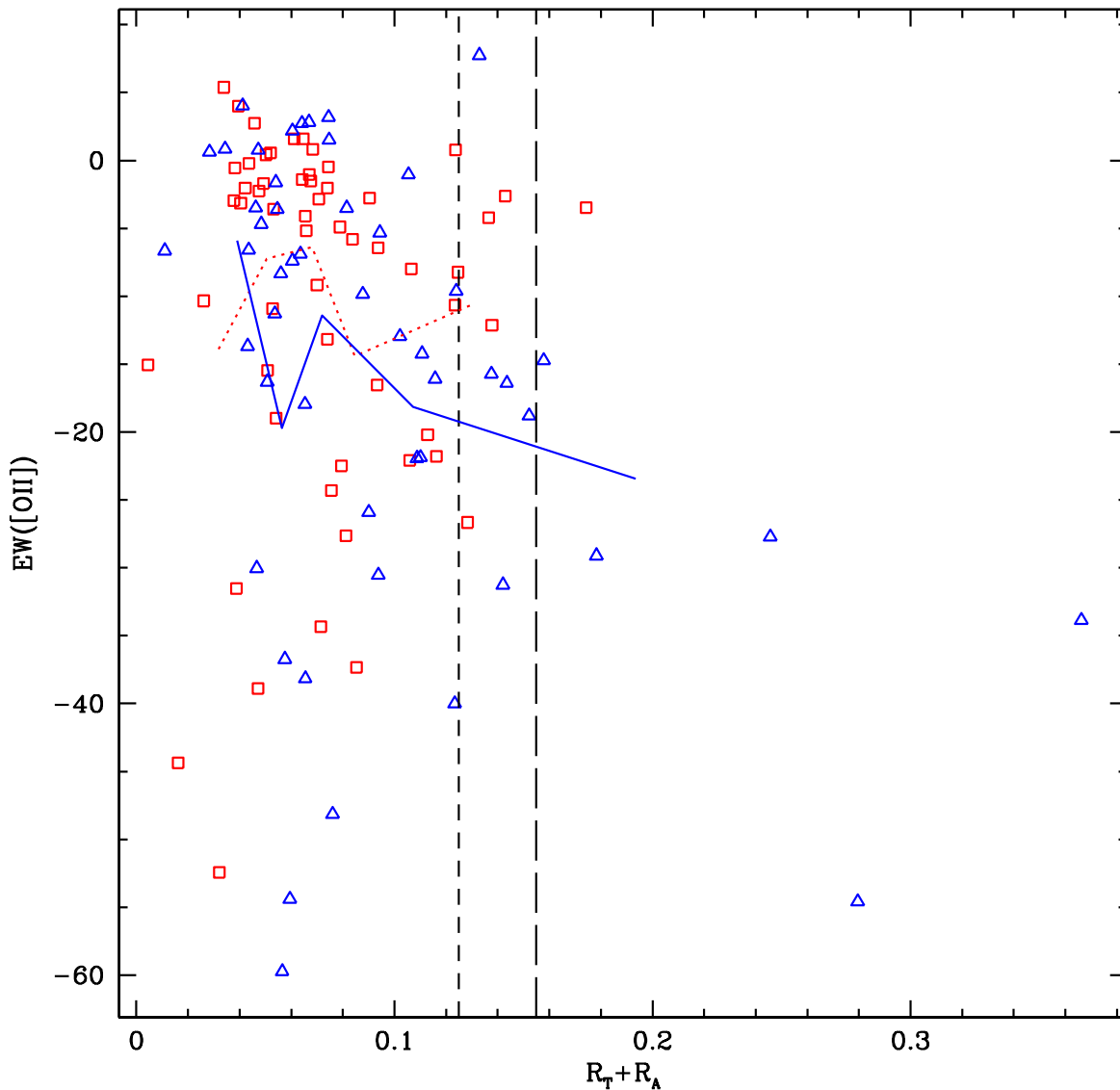


Fig. 15.— [OII]3727 equivalent width is plotted versus asymmetry for paired (blue triangles) and isolated (red squares) galaxies. Galaxies to the right of the short-dashed line are described as being “asymmetric”; those to the right of the long-dashed line are “strongly asymmetric”. The dotted red line gives the mean $EW([OII])$ of isolated galaxies in five bins of $R_T + R_A$, while the solid blue line gives the mean $EW([OII])$ of paired galaxies. Paired and isolated galaxies have similar distributions in the symmetric regime. Most of the asymmetric galaxies have strong emission and are found in pairs.

Table 1: Properties of Galaxy Pairs.

HST Target	Mean Redshift	θ (arcsec)	r_p (h^{-1} kpc)	Δv (km/s)	ΔM_R (mag)
01	0.13339	11.5	17.9	103	2.2
04	0.26693	5.1	13.0	232	1.8
05	0.47185	2.2	7.7	20	2.0
06	0.35090	4.0	12.0	133	1.2
07	0.27009	2.5	6.4	319	0.2
09	0.38407	2.0	6.2	63	1.3
10	0.29829	2.1	5.8	162	1.5
11	0.27099	7.0	18.0	189	0.8
13	0.29901	7.0	19.2	201	0.4
14	0.40769	3.2	10.4	264	1.6
15	0.30960	1.3	3.6	82	0.4
16	0.14997	6.4	11.0	76	0.4
20	0.39666	1.8	5.8	101	0.6
25	0.19171	8.6	17.7	423	2.4
28	0.24645	2.1	5.1	284	2.2
29	0.13640	7.6	12.1	193	0.6
30	0.19029	6.8	13.8	360	0.4
31	0.39017	1.7	5.5	50	1.4
34	0.32471	2.4	7.0	29	0.6
35	0.20435	9.2	19.8	50	0.0
36	0.39208	2.4	7.6	198	0.0
38	0.38954	6.0	18.9	179	0.9
39	0.42721	3.8	12.5	78	1.0
40	0.55648	5.5	20.5	112	0.4
45	0.14608	5.6	9.4	5	2.4
46	0.26193	6.9	17.4	404	2.1
49	0.26965	2.9	7.5	172	1.7
51	0.34926	1.9	5.6	138	0.9
52	0.36420	5.0	15.3	171	0.5
60	0.51024	3.6	13.0	44	0.1
65	0.14744	2.4	4.1	133	0.6
67	0.19767	8.4	17.6	48	1.1
68	0.40839	4.7	15.2	143	1.9
70	0.29718	7.1	19.4	42	1.0
72	0.50631	2.1	7.5	125	0.4

Table 2: Catalog of Paired Galaxies.

HST ID	CNOC2 Name	RA (J2000)	Dec (J2000)	z	R_C	M_R	B/T	R_T+R_A	$(B-R)_0$	[OII] E.W.
01A	0223-100810	02:26:53.50	00:02:48.0	0.13358	17.0	-21.2	0.69	0.04	1.52	—
01B	0223-100778	02:26:53.07	00:02:38.6	0.13319	19.2	-19.0	0.67	0.08	1.18	—
04A	0223-140091	02:25:22.94	00:07:12.4	0.26742	18.8	-20.9	0.01	0.25	0.84	-27.7
04B	0223-140075	02:25:23.20	00:07:09.2	0.26644	20.6	-19.1	0.46	0.09	0.90	-25.9
05A	0223-062160	02:25:50.10	01:00:41.5	0.47190	18.8	-22.9	0.58	0.06	1.76	2.2
05B	0223-062166	02:25:50.25	01:00:42.0	0.47180	20.1	-20.9	0.40	0.06	2.81	2.7
06A	0223-130708	02:25:09.06	00:18:05.2	0.35060	19.0	-21.7	0.48	0.03	1.50	0.6
06B	0223-130707	02:25:09.33	00:18:04.8	0.35120	20.1	-20.5	0.38	0.04	1.72	-13.7
07A	0223-191878	02:23:28.45	-00:03:55.1	0.27077	19.2	-20.5	0.00	0.11	0.93	-21.9
07B	0223-191879	02:23:28.29	-00:03:55.0	0.26942	19.6	-20.2	0.01	0.10	0.89	-13.0
09A	0223-121099	02:26:17.22	00:12:46.9	0.38393	19.4	-21.5	0.33	0.06	1.65	-6.9
09B	0223-121101	02:26:17.09	00:12:47.3	0.38422	20.6	-20.2	0.66	0.07	1.00	2.8
10A	0223-030307	02:25:49.16	00:30:33.1	0.29864	19.1	-21.1	0.48	0.06	1.43	-54.4
10B	0223-030309	02:25:49.02	00:30:33.7	0.29794	20.4	-19.6	0.00	0.08	0.84	-48.2
11A	0223-050675	02:25:55.13	00:47:18.6	0.27059	19.6	-20.2	0.18	0.11	1.07	-14.2
11B	0223-050679	02:25:55.59	00:47:18.9	0.27139	20.5	-19.4	0.38	0.06	1.15	-7.4
13A	0223-030266	02:25:49.87	00:30:23.7	0.29945	19.5	-20.7	0.21	0.11	1.32	-21.9
13B	0223-030259	02:25:49.42	00:30:21.9	0.29858	19.9	-20.3	0.44	0.06	1.30	-8.3
14A	0223-031099	02:25:48.86	00:34:00.2	0.40831	19.6	-20.9	0.08	0.28	0.69	-54.6
14B	0223-031118	02:25:48.90	00:34:03.4	0.40707	21.1	-19.3	0.40	0.06	0.37	-59.7
15A	0223-131144	02:25:25.89	00:20:06.4	0.30978	20.0	-20.4	0.59	0.05	1.39	-3.5
15B	0223-131141	02:25:25.82	00:20:05.8	0.30942	20.2	-20.0	1.00	0.11	1.56	-1.0
16A	0223-160751	02:25:02.42	00:01:13.1	0.15011	20.0	-18.3	0.01	0.05	0.77	—
16B	0223-160754	02:25:02.84	00:01:14.4	0.14982	20.4	-17.9	0.32	0.04	0.74	—
20A	0223-040345	02:26:13.19	00:38:25.3	0.39643	20.1	-20.4	0.00	0.37	0.81	-33.9
20B	0223-040350	02:26:13.24	00:38:26.9	0.39690	20.7	-19.9	0.07	0.05	0.79	-30.0
25A	0920-010722	09:24:03.22	37:04:52.4	0.19087	17.1	-22.0	1.00	0.07	1.70	—
25B	0920-010688	09:24:03.32	37:04:43.9	0.19255	19.5	-19.6	0.00	0.13	1.55	—
28A	0920-081315	09:24:39.40	37:08:15.3	0.24586	18.2	-21.6	0.67	0.05	1.55	-3.6
28B	0920-081301	09:24:39.46	37:08:13.4	0.24704	20.4	-19.3	0.48	0.09	1.65	-9.8
29A	0920-050264	09:23:43.09	37:31:42.9	0.13676	18.6	-19.7	0.86	0.11	1.47	—
29B	0920-050258	09:23:42.49	37:31:40.2	0.13603	19.0	-19.1	0.00	0.29	0.69	—
30A	0920-010879	09:24:08.24	37:05:42.5	0.18958	18.8	-20.3	0.73	0.11	1.45	—
30B	0920-010860	09:24:07.95	37:05:36.8	0.19101	19.2	-19.9	0.80	0.04	1.56	—
31A	0920-131238	09:23:12.63	37:07:04.7	0.39028	18.9	-22.1	0.53	0.05	1.67	-1.6
31B	0920-131230	09:23:12.50	37:07:04.0	0.39005	20.4	-20.7	0.46	0.07	1.69	1.5

Table 2: Catalog of Paired Galaxies – *continued*.

HST ID	CNOC2 Name	RA (J2000)	Dec (J2000)	z	R_C	M_R	B/T	R_T+R_A	$(B-R)_0$	[OII] E.W.
34A	0920-020557	09:23:30.71	37:11:19.6	0.32477	19.6	-20.6	0.01	0.18	0.83	-29.1
34B	0920-020566	09:23:30.87	37:11:21.0	0.32464	20.1	-20.0	0.00	0.15	0.63	-18.8
35A	0920-020237	09:24:06.44	37:09:45.3	0.20425	19.7	-19.4	0.16	0.16	0.98	—
35B	0920-020209	09:24:05.90	37:09:38.8	0.20445	19.7	-19.4	0.02	0.11	1.16	—
36A	0920-160826	09:22:27.87	36:46:51.9	0.39162	19.9	-21.0	0.30	0.05	1.24	-4.7
36B	0920-160832	09:22:27.83	36:46:54.2	0.39254	20.0	-21.0	0.80	0.04	1.61	-6.6
38A	0920-150212	09:23:13.80	36:45:29.3	0.38996	20.2	-20.9	0.60	0.05	1.68	0.8
38B	0920-150213	09:23:14.30	36:45:29.5	0.38913	21.0	-20.0	0.76	0.03	1.36	0.8
39A	0920-151065	09:23:00.43	36:49:45.3	0.42740	20.3	-21.1	0.72	0.13	1.83	7.8
39B	0920-151064	09:23:00.12	36:49:45.2	0.42703	21.2	-20.1	0.71	0.01	1.65	-6.6
40A	0920-180867	09:21:42.11	36:37:57.4	0.55677	20.7	-21.2	0.35	0.12	1.08	-16.1
40B	0920-180845	09:21:42.49	36:37:54.4	0.55619	20.7	-21.6	0.44	0.07	1.53	3.2
45A	1447-101867	14:50:25.13	08:56:28.0	0.14609	18.1	-20.2	0.13	0.19	0.92	—
45B	1447-101865	14:50:25.48	08:56:25.8	0.14607	20.4	-17.8	0.00	0.13	0.44	—
46A	1447-140046	14:48:55.81	08:56:44.4	0.26108	18.2	-21.6	0.05	0.12	1.09	-9.6
46B	1447-140054	14:48:56.27	08:56:45.7	0.26278	20.3	-19.4	0.02	0.05	1.03	-16.3
49A	1447-110843	14:49:26.91	08:52:11.1	0.27002	19.1	-20.7	0.05	0.12	0.98	—
49B	1447-110838	14:49:27.10	08:52:10.2	0.26929	20.8	-19.0	0.00	0.14	1.15	-16.4
51A	1447-051065	14:49:55.08	09:38:44.9	0.34895	19.2	-21.5	0.86	0.05	1.75	-11.3
51B	1447-051056	14:49:54.98	09:38:43.7	0.34957	20.0	-20.6	0.77	0.16	1.26	-14.7
52A	1447-082155	14:50:05.66	09:11:52.5	0.36381	19.3	-21.1	0.06	0.14	0.82	-15.7
52B	1447-082172	14:50:05.87	09:11:56.3	0.36459	20.1	-20.6	0.23	0.09	1.15	-5.3
60A	1447-040704	14:49:38.98	09:29:31.0	0.51035	20.9	-20.6	0.60	0.04	0.68	4.0
60B	1447-040709	14:49:38.74	09:29:31.0	0.51013	21.3	-20.4	0.09	0.07	1.24	-18.0
65A	2148-042181	21:51:24.69	-05:07:10.2	0.14719	18.8	-19.7	0.56	0.05	1.34	—
65B	2148-042170	21:51:24.76	-05:07:12.4	0.14770	19.3	-19.1	0.08	0.13	1.12	—
67A	2148-031553	21:51:12.48	-05:17:42.8	0.19758	19.1	-19.9	0.69	0.18	0.77	—
67B	2148-031529	21:51:12.88	-05:17:48.6	0.19777	20.2	-18.7	0.04	0.06	0.91	—
68A	2148-071349	21:51:22.15	-04:45:14.3	0.40806	19.5	-21.6	0.27	0.08	1.58	-3.5
68B	2148-071332	21:51:22.09	-04:45:18.9	0.40873	21.1	-19.7	0.01	0.07	0.97	-38.1
70A	2148-051930	21:51:26.12	-04:58:16.6	0.29727	20.0	-19.9	0.10	0.09	0.88	-30.5
70B	2148-051898	21:51:25.97	-04:58:23.3	0.29709	21.1	-18.9	0.61	0.06	1.15	-36.7
72A	2148-162261	21:50:16.57	-05:45:45.8	0.50600	20.8	-20.4	0.19	0.12	0.56	-40.0
72B	2148-162264	21:50:16.46	-05:45:44.4	0.50663	21.2	-20.0	0.23	0.14	0.81	-31.2

Table 3: Catalog of Isolated Galaxies.

HST ID	CNOC2 Name	RA (J2000)	Dec (J2000)	z	R_C	M_R	B/T	R_T+R_A	$(B-R)_0$	[OII] E.W.
01	0223-100974	02:26:48.44	00:03:40.0	0.57410	21.0	-20.9	0.02	0.07	0.80	-5.2
02	0223-100908	02:26:47.44	00:03:19.9	0.16531	21.2	-17.4	0.12	0.06	0.75	—
03	0223-100681	02:26:52.15	00:02:12.2	0.23069	19.2	-20.4	0.56	0.07	1.34	-9.2
04	0223-020713	02:25:50.07	00:25:12.0	0.37752	20.5	-20.4	0.28	0.09	1.41	-2.8
05	0223-140376	02:25:25.74	00:08:32.8	0.28505	20.0	-20.1	0.50	0.05	1.36	-19.0
06	0223-140073	02:25:15.60	00:07:06.9	0.61474	20.8	-21.0	0.00	0.13	0.91	-26.7
07	0223-062315	02:25:52.53	01:01:24.2	0.30465	19.2	-21.1	0.91	0.05	1.55	-3.6
08	0223-070252	02:25:52.40	01:02:17.8	0.30533	19.8	-20.4	0.45	0.12	1.35	—
09	0223-130667	02:25:12.65	00:17:54.5	0.35944	18.8	-21.9	0.46	0.05	1.49	0.4
10	0223-130491	02:25:12.74	00:17:06.4	0.29227	19.1	-21.0	0.52	0.05	1.47	0.6
11	0223-130656	02:25:13.25	00:17:51.7	0.30653	19.4	-20.9	0.75	0.12	1.67	0.8
12	0223-130882	02:25:11.73	00:18:50.4	0.39001	20.4	-20.7	0.79	0.07	1.75	-1.0
13	0223-191602	02:23:25.41	-00:04:49.1	0.24321	20.2	-19.3	0.07	0.08	1.04	-22.5
14	0223-191492	02:23:25.12	-00:05:07.9	0.27001	20.5	-19.5	0.45	0.11	1.63	-22.1
15	0223-030382	02:25:51.62	00:30:51.3	0.29849	19.6	-20.6	0.73	0.05	1.51	-15.4
16	0223-021797	02:25:47.12	00:29:26.3	0.36418	19.2	-21.6	0.76	0.04	1.63	-3.1
17	0223-030996	02:25:45.61	00:33:33.4	0.30046	21.0	-18.9	0.02	0.04	0.82	-31.5
18	0223-131066	02:25:31.36	00:19:42.4	0.36261	20.3	-20.2	0.05	0.03	1.01	-10.3
19	0223-161138	02:25:06.88	00:02:32.8	0.33161	20.3	-20.2	0.50	0.04	1.43	4.0
20	0223-040234	02:26:19.19	00:37:56.7	0.26701	19.7	-20.1	0.01	0.11	0.94	-8.0
21	0223-040342	02:26:11.95	00:38:24.1	0.18752	18.5	-20.4	0.03	0.11	0.89	—
22	0223-031673	02:26:05.17	00:36:25.5	0.42483	21.2	-19.7	0.00	0.12	0.91	-21.8
23	0223-171157	02:24:53.29	-00:06:20.5	0.38609	20.6	-20.0	0.10	0.08	0.91	-24.3
24	0223-170849	02:24:50.90	-00:07:12.7	0.39019	21.2	-19.4	0.10	0.02	0.91	-44.4
25	0223-170801	02:24:47.75	-00:07:21.9	0.29572	19.6	-20.5	0.01	0.14	1.17	-4.2
26	0223-171287	02:24:42.76	-00:05:57.8	0.55464	20.5	-21.8	0.49	0.06	1.76	1.6
27	0920-010390	09:24:05.97	37:03:27.6	0.37363	19.6	-21.4	0.51	0.04	1.68	-2.9
28	0920-010331	09:24:06.23	37:03:09.7	0.37234	20.3	-20.6	0.63	0.03	1.71	5.4
29	0920-010500	09:24:03.30	37:03:53.7	0.19309	20.6	-18.2	0.06	0.02	0.82	—
30	0920-010748	09:24:04.19	37:04:59.4	0.20159	18.4	-20.8	0.57	0.04	1.59	—
31	0920-080744	09:24:10.53	37:05:24.4	0.32611	19.8	-20.8	0.44	0.12	1.39	-8.2
32	0920-081152	09:24:40.62	37:07:32.7	0.24619	20.4	-19.4	0.04	0.11	2.05	—
33	0920-050330	09:23:43.87	37:32:02.2	0.24630	19.4	-20.3	0.44	0.09	1.44	—
34	0920-050346	09:23:52.14	37:32:07.0	0.32093	20.6	-19.8	0.53	0.04	1.55	—
35	0920-011194	09:24:04.30	37:07:04.7	0.23134	18.7	-20.9	0.63	0.04	1.58	-0.6
36	0920-011167	09:24:08.27	37:06:55.3	0.37291	19.0	-21.9	0.93	0.04	1.65	-2.0
37	0920-131204	09:23:13.70	37:06:56.7	0.39211	18.8	-22.2	0.66	0.07	1.62	0.8
38	0920-131311	09:23:20.06	37:07:21.6	0.24337	18.3	-21.4	0.58	0.04	1.53	-0.2
39	0920-131351	09:23:21.04	37:07:31.1	0.24503	20.1	-19.5	0.21	0.05	0.99	-38.9

Table 3: Catalog of Isolated Galaxies – *continued*.

HST ID	CNOC2 Name	RA (J2000)	Dec (J2000)	z	R_C	M_R	B/T	R_T+R_A	$(B - R)_0$	[OII] E.W.
40	0920-020409	09:23:33.83	37:10:39.4	0.24740	18.1	-21.6	0.44	0.07	1.62	-0.5
41	0920-020268	09:23:31.84	37:09:55.6	0.24656	18.4	-21.1	0.04	0.14	1.22	-2.6
42	0920-081330	09:24:12.56	37:08:22.9	0.46150	19.9	-21.7	0.32	0.06	2.20	1.6
43	0920-020299	09:24:07.39	37:10:01.3	0.24655	20.0	-19.7	0.53	0.05	1.51	2.7
44	0920-160943	09:22:34.01	36:47:14.5	0.11019	17.4	-20.3	0.61	0.14	2.22	—
45	0920-150040	09:23:13.93	36:44:43.1	0.44119	20.8	-20.3	0.28	0.00	0.93	-15.1
46	0920-150181	09:23:15.54	36:45:20.7	0.18807	19.6	-19.3	0.03	0.06	1.01	—
47	0920-150193	09:23:23.48	36:45:25.5	0.55982	20.3	-21.4	0.06	0.07	0.92	-13.2
48	0920-151228	09:22:56.31	36:50:33.4	0.42814	20.8	-20.5	0.65	0.07	1.52	-2.9
49	0920-180260	09:21:45.07	36:36:29.9	0.46012	20.8	-20.3	0.07	0.12	0.76	-10.7
50	0920-181107	09:21:44.43	36:38:30.9	0.43685	20.0	-21.2	0.06	0.09	1.32	-6.4
51	0920-030026	09:23:40.18	37:16:05.2	0.32032	20.7	-19.4	0.00	0.14	1.85	-12.2
52	1447-101860	14:50:24.79	08:56:23.9	0.37270	20.4	-20.4	0.40	0.07	1.29	-1.5
53	1447-151214	14:48:53.47	08:55:20.0	0.51551	21.3	-19.8	0.07	0.07	0.65	—
54	1447-110526	14:49:25.59	08:50:52.9	0.60697	19.7	-22.2	0.14	0.17	0.95	-3.5
55	1447-110482	14:49:28.21	08:50:37.6	0.37317	20.9	-19.6	0.02	0.08	0.94	-27.6
56	1447-110595	14:49:29.40	08:51:07.8	0.55393	21.1	-20.5	0.01	0.09	0.65	-37.3
57	1447-051337	14:49:52.34	09:39:47.5	0.43315	20.6	-20.6	0.24	0.07	1.18	-34.3
58	1447-082395	14:50:01.48	09:12:43.2	0.30347	18.9	-21.5	1.00	0.07	1.54	-4.1
59	1447-040758	14:49:34.82	09:29:43.1	0.13114	20.1	-18.0	0.28	0.07	0.90	—
60	1447-040497	14:49:38.34	09:28:34.9	0.40724	20.1	-20.7	0.02	0.08	0.66	-5.8
61	1447-040441	14:49:40.07	09:28:23.0	0.46205	20.6	-20.9	0.67	0.05	1.46	-2.3
62	2148-070517	21:51:09.61	-04:47:50.4	0.15444	17.8	-20.8	0.80	0.08	1.65	—
63	2148-191639	21:48:47.50	-05:57:32.6	0.25759	19.2	-20.4	0.40	0.09	0.98	-16.6
64	2148-191186	21:48:47.92	-05:59:02.3	0.15252	19.8	-18.5	0.00	0.09	0.76	—
65	2148-191213	21:48:47.63	-05:58:56.9	0.55673	21.1	-21.0	0.81	0.09	2.04	—
66	2148-042309	21:51:19.50	-05:06:47.8	0.54593	21.5	-19.8	0.00	0.03	0.66	-52.4
67	2148-042026	21:51:25.10	-05:07:42.4	0.14776	17.3	-21.1	0.43	0.07	1.53	—
68	2148-031234	21:51:12.94	-05:18:43.6	0.73200	20.2	-21.7	0.32	0.14	0.39	—
69	2148-071573	21:51:20.96	-04:44:38.2	0.28803	19.7	-20.4	0.99	0.06	1.53	-1.4
70	2148-071141	21:51:18.04	-04:45:55.9	0.12729	17.7	-20.3	0.04	0.09	0.94	—
71	2148-071059	21:51:18.02	-04:46:09.0	0.28720	18.3	-21.8	0.81	0.05	1.75	-1.7
72	2148-070881	21:51:20.76	-04:46:38.5	0.53628	20.9	-20.7	0.18	0.05	1.00	-10.9
73	2148-051766	21:51:31.74	-04:59:00.3	0.15642	20.5	-17.9	0.09	0.12	0.76	—
74	2148-161891	21:50:19.89	-05:47:13.0	0.14443	19.8	-18.5	0.61	0.11	0.94	—
75	2148-162029	21:50:20.47	-05:46:39.3	0.37508	19.9	-20.9	0.37	0.07	1.30	-2.0
76	2148-162168	21:50:18.51	-05:46:06.5	0.31699	20.6	-19.7	0.12	0.08	1.14	-4.9
77	2148-162322	21:50:19.63	-05:45:30.1	0.39176	21.5	-19.1	0.05	0.11	0.81	-20.2

Table 4: Comparison of Paired and Isolated Galaxies.

Property	Paired	Isolated	KS Prob (%)
N	70	77	
z	0.31 ± 0.01	0.34 ± 0.02	66
R_C	19.8 ± 0.1	19.9 ± 0.1	44
M_R	-20.3 ± 0.1	-20.4 ± 0.1	47
$(B - R)_0$	1.20 ± 0.05	1.27 ± 0.05	66
B/T	0.36 ± 0.04	0.35 ± 0.03	95
$R_T + R_A$	0.098 ± 0.008	0.076 ± 0.004	16
$[OII]EW$	-15.8 ± 2.3	-10.5 ± 1.7	11